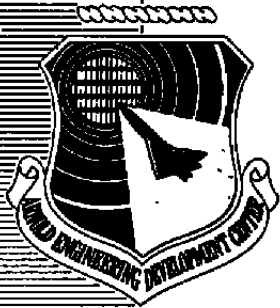


**AEDC-TR-85-30**  
**VOL. I (Revised)**



# Analysis and Verification of the Icing Scaling Equations

Analysis and Verification

Gary A. Ruff  
Sverdrup Technology, Inc.

~~PROPERTY OF U.S. AIR FORCE~~  
~~AEDC TECHNICAL LIBRARY~~

March 1986

Final Report for Period August 1, 1981 through March 31, 1984

~~TECHNICAL REPORTS~~  
~~FILE COPY~~

Approved for public release; distribution unlimited.

**ARNOLD ENGINEERING DEVELOPMENT CENTER**  
**ARNOLD AIR FORCE STATION, TENNESSEE**  
**AIR FORCE SYSTEMS COMMAND**  
**UNITED STATES AIR FORCE**

## NOTICES

When U. S. Government drawings, specifications, or other data are used for any purpose other than a definitely related Government procurement operation, the Government thereby incurs no responsibility nor any obligation whatsoever, and the fact that the government may have formulated, furnished, or in any way supplied the said drawings, specifications, or other data, is not to be regarded by implication or otherwise, or in any manner licensing the holder or any other person or corporation, or conveying any rights or permission to manufacture, use, or sell any patented invention that may in any way be related thereto.

Qualified users may obtain copies of this report from the Defense Technical Information Center.

References to named commercial products in this report are not to be considered in any sense as an endorsement of the product by the United States Air Force or the Government.

This report has been reviewed by the Office of Public Affairs (PA) and is releasable to the National Technical Information Service (NTIS). At NTIS, it will be available to the general public, including foreign nations.

## APPROVAL STATEMENT

This report has been reviewed and approved.



DAVID A. DUESTERHAUS  
Directorate of Technology  
Deputy for Operations

Approved for publication:

FOR THE COMMANDER



LOWELL C. KEEL, Lt Colonel, USAF  
Director of Technology  
Deputy for Operations

UNCLASSIFIED

SECURITY CLASSIFICATION OF THIS PAGE

REPORT DOCUMENTATION PAGE

1a REPORT SECURITY CLASSIFICATION <b>UNCLASSIFIED</b>		1b RESTRICTIVE MARKINGS	
2a SECURITY CLASSIFICATION AUTHORITY		3 DISTRIBUTION/AVAILABILITY OF REPORT See Reverse of This Page.	
2b DECLASSIFICATION/DOWNGRADING SCHEDULE			
4. PERFORMING ORGANIZATION REPORT NUMBER(S) AEDC-TR-85-30, Vol. I (Revised)		5 MONITORING ORGANIZATION REPORT NUMBER(S)	
6a. NAME OF PERFORMING ORGANIZATION Arnold Engineering Development Center	6b. OFFICE SYMBOL (If applicable) DOT	7a. NAME OF MONITORING ORGANIZATION	
6c. ADDRESS (City, State and ZIP Code) Air Force Systems Command Arnold Air Force Station, TN 37389-5000		7b. ADDRESS (City, State and ZIP Code)	
8a. NAME OF FUNDING/SPONSORING ORGANIZATION Arnold Engineering Development Center	8b. OFFICE SYMBOL (If applicable) DO	9. PROCUREMENT INSTRUMENT IDENTIFICATION NUMBER	
8c. ADDRESS (City, State and ZIP Code) Air Force Systems Command Arnold Air Force Station, TN 37389-5000		10 SOURCE OF FUNDING NOS.	
11. TITLE (Include Security Classification) See Reverse of This Page.		PROGRAM ELEMENT NO. 921E06 65807F	PROJECT NO.
		TASK NO.	WORK UNIT NO.
12. PERSONAL AUTHOR(S) Ruff, Gary A., Sverdrup Technology, Inc., AEDC Group			
13a. TYPE OF REPORT Final	13b. TIME COVERED FROM 8/1/81 TO 3/31/84	14 DATE OF REPORT (Yr., Mo., Day) March 1986	15 PAGE COUNT 81
16. SUPPLEMENTARY NOTATION Available in Defense Technical Information Center (DTIC).			
17 COSATI CODES		18. SUBJECT TERMS (Continue on reverse if necessary and identify by block number)	
FIELD	GROUP	scaling thermal model	
14	02	airfoil icing	
19	02		
19. ABSTRACT (Continue on reverse if necessary and identify by block number) The aerodynamics and thermodynamics of the ice-accretion process were evaluated to identify parameters that could scale ice accretions from full-scale vehicles to sub-scale models. Experimental data obtained from application of these scaling parameters resulted in the verification of a set of icing scaling equations. Scaling parameter derivation, validation, behavior, and limitations are presented.			
20. DISTRIBUTION/AVAILABILITY OF ABSTRACT UNCLASSIFIED/UNLIMITED <input type="checkbox"/> SAME AS RPT <input checked="" type="checkbox"/> DTIC USERS <input type="checkbox"/>		21. ABSTRACT SECURITY CLASSIFICATION UNCLASSIFIED	
22a. NAME OF RESPONSIBLE INDIVIDUAL W. O. Cole		22b TELEPHONE NUMBER (Include Area Code) (615)454-7813	22c OFFICE SYMBOL DOS

UNCLASSIFIED

SECURITY CLASSIFICATION OF THIS PAGE

3. DISTRIBUTION/AVAILABILITY OF REPORT

Approved for public release; distribution unlimited.

11. TITLE

Analysis and Verification of the Icing Scaling Equations, Vol. I—Analysis and Verification

UNCLASSIFIED

SECURITY CLASSIFICATION OF THIS PAGE

## **PREFACE**

The work reported herein was conducted by the Arnold Engineering Development Center (AEDC), Air Force Systems Command (AFSC) at the request of AEDC/DOT. The Air Force Project Manager was Mr. D. A. Duesterhaus. The results were obtained by Sverdrup Technology, Inc., AEDC Group, operating contractor for aeropropulsion testing at the AEDC, AFSC, Arnold Air Force Station, Tennessee, under Project Number D188EW. The experimental analysis was performed from August 1981 to October 1983, and the analytical analysis was completed in March 1984. The manuscript was submitted for publication on March 21, 1985.

Volume I contains the analysis and evaluation of the icing scaling equations, whereas Volume II is a description and listing of the computer code entitled "SIMICE."

## CONTENTS

	<u>Page</u>
1.0 INTRODUCTION .....	7
1.1 Background .....	7
1.2 Scope of Investigation .....	7
1.3 Outline of Report .....	8
2.0 DISCUSSION OF ICING SCALING .....	8
2.1 Definition .....	8
2.2 Types of Icing Scaling .....	9
2.3 Icing Scaling Requirements .....	9
3.0 IDENTIFICATION OF THE SCALING PARAMETERS .....	10
3.1 Flow Field Scaling Requirements .....	10
3.2 Droplet Trajectory Scaling Requirements .....	11
3.3 Total Water-Catch Scaling Requirements .....	18
3.4 Thermodynamic Scaling Requirements .....	19
4.0 SCALING METHODS INVESTIGATED .....	30
4.1 Past Scaling Investigations .....	30
4.2 Identification of the Scaling Methods .....	30
4.3 Solution of the Scaling Equations .....	31
5.0 EXPERIMENTAL VERIFICATION .....	32
5.1 Scaling Test Procedures .....	32
5.2 Facility Description .....	33
5.3 Test Procedures .....	37
5.4 Test Results .....	38
6.0 ICING SCALING APPLICATIONS .....	49
6.1 Sample Scaling Problems .....	49
7.0 LIMITATIONS .....	57
7.1 Velocity Scaling Limitations .....	57
7.2 General Limitations .....	59
8.0 SUMMARY OF RESULTS .....	60
REFERENCES .....	61

## ILLUSTRATIONS

### Figure

1. Definition of Total and Local Collection Efficiency .....	12
2. Total Collection Efficiency versus Inertia Parameter for a Cylinder .....	13

<u>Figure</u>	<u>Page</u>
3. Stagnation-Point Collection Efficiency versus Inertia Parameter for a Cylinder .....	13
4. Droplet Impingement Limit versus Inertia Parameter for a Cylinder .....	14
5. Total Collection Efficiency versus Modified Inertia Parameter for Various Geometries .....	15
6. Effect of Velocity, Static Pressure, and Model Size on the Mass Median Droplet Diameter for a Constant Value of Modified Inertia Parameter, $K_0$ .....	16
7. Comparison of Local Collection Efficiency Calculations Using Monodispersed and Multidispersed Droplet Distributions .....	17
8. Effect of Velocity and Model Size on the Icing Time for a Constant Value of Accumulation Parameter, $A_c$ .....	20
9. Comparison of Measured and Calculated Surface Temperatures in Incipient Icing Conditions .....	23
10. Examples of Ice Accretions Formed at Various Values of Stagnation-Point Freezing Fraction .....	24
11. Effect of Velocity, Static Pressure, and Static Temperature on LWC for a Constant Value of Freezing Fraction, $n$ .....	25
12. Effect of Velocity, Static Pressure, and Model Size on LWC for a Constant Value of Relative Heat Factor, $b$ .....	26
13. Effect of Velocity on Static Temperature for a Constant Value of Droplet Energy Potential, $\phi$ .....	28
14. Effect of Velocity and Static Temperature on Static Pressure for a Constant Value of Air Energy Potential, $\theta$ .....	29
15. Example of Test Cell and Ice-Accretion Measurement Repeatability .....	34
16. Supercritical Airfoil Section Used in the Icing Scaling Studies .....	34
17. Icing Research Test Cell .....	35
18. Fiber-Optics Particle-Sizing System .....	36
19. Comparison of FOS Data with Spray Nozzle Calibration .....	36
20. Comparison of Input and Measured LWC in the Research Test Cell .....	37
21. Comparison of Rime, Mixed, and Glaze Ice-Accretion Scaling Using Method 1 to Establish the Experimental Similitude Conditions .....	39

<u>Figure</u>	<u>Page</u>
22. Comparison of Glaze and Mixed Ice-Accretion Scaling Using Method 2 to Establish the Experimental Similitude Conditions .....	41
23. Comparison of Glaze and Mixed Ice-Accretion Scaling Using Method 3 to Establish the Experimental Similitude Conditions .....	43
24. Comparison of Glaze and Mixed Ice-Accretion Scaling Using Method 4 to Establish the Experimental Similitude Conditions .....	45
25. Sample Problem 1: Static Temperature of the Model Condition as a Function of Model Velocity for a Constant Value of Droplet Energy Potential, $\phi$ .....	50
26. Sample Problem 1: Static Pressure of the Model Condition as a Function of Model Velocity for a Constant Value of Air Energy Potential, $\theta$ .....	51
27. Sample Problem 1: LWC of the Model Condition as a Function of Model Velocity for a Constant Value of Freezing Fraction, $n$ .....	52
28. Sample Problem 1: Mass Median Droplet Diameter of the Model Condition as a Function of Model Velocity for a Constant Value of Modified Inertia Parameter, $K_0$ .....	53
29. Sample Problem 1: Icing Time of the Model Condition as a Function of Model Velocity for a Constant Value of Accumulation Parameter, $A_c$ .....	54
30. Sample Problem 2: Total Pressure of the Model Condition as a Function of Model Velocity for a Constant Value of Air Energy Potential, $\theta$ .....	55
31. Sample Problem 2: LWC of the Model Condition as a Function of Model Velocity for a Constant Value of Freezing Fraction, $n$ .....	55
32. Sample Problem 2: Mass Median Droplet Diameter of the Model Condition as a Function of Model Velocity for a Constant Value of Modified Inertia Parameter, $K_0$ .....	56
33. Sample Problem 2: Icing Time of the Model Conditon as a Function of Model Velocity for a Constant Value of Accumulation Parameter, $A_c$ .....	56
34. Definition of Icing Shedding Analysis Terms .....	58



<u>Table</u>	<u>Page</u>
--------------	-------------

**TABLES**

1. Summary of Past Scaling Investigations .....	30
2. Summary of the Scaling Methods Investigated at the AEDC .....	32
3. Ranges of Test Parameters Investigated at the AEDC .....	59

**APPENDIXES**

A. Derivation of the Modified Inertia Parameter .....	63
B. Derivation of the Icing Energy Equation .....	66

NOMENCLATURE .....	74
--------------------	----

## **1.0 INTRODUCTION**

### **1.1 BACKGROUND**

The formation of ice on aircraft surfaces occurs during flight through supercooled droplets. Ice accretions on these surfaces usually degrade both aircraft performance and operational safety. For this reason, it has become important in the design and certification phases of system development to evaluate system performance degradation because of icing.

The most acceptable method of evaluating the performance characteristics of aircraft and aircraft components for system certification would be to conduct flight tests in natural icing conditions. Adequate system evaluation through icing flight tests requires specific weather conditions, posing severe operational limitations because of the low frequency of their occurrence. This makes certification through flight testing time consuming and expensive because large amounts of flying time are required to adequately evaluate a system over a wide range of conditions. Flight testing in a simulated cloud produced by an icing tanker would appear to be the next most desirable method of conducting icing tests. In practice, this method of flight testing is severely limited by tanker operational limitations, lack of control of atmospheric parameters such as temperature, pressure and humidity, and the logistics of maintaining steady flight in a cloud produced by a leading aircraft. Therefore, ground testing in altitude facilities has become an accepted approach for evaluating aircraft system performance in icing conditions.

The size of many of the aircraft components to be tested greatly limits the number of test facilities capable of conducting icing tests. It would be beneficial to the icing community if the feasibility of using scale models in these tests could be proven. The problem is complicated because the icing process is governed by the impingement of water droplets and the thermodynamics of the freezing process on the surface. This document gives the results of a study conducted at Arnold Engineering Development Center (AEDC) Engine Test Facility (ETF) to experimentally verify a set of icing scaling equations.

### **1.2 SCOPE OF INVESTIGATION**

A research program was conducted at the AEDC/ETF to evaluate the icing scaling requirements. The objectives of the study were (1) to evaluate the equations governing the icing process to identify proposed scaling parameters, (2) to develop a computer code to solve the various forms of the icing scaling equations, (3) to conduct tests to determine which, if any, of the proposed methods produced scale ice accretions, and (4) if an accurate set of icing scaling equations were found, to write a final computer code that could be used in icing tests.

The scaling verification tests were conducted using full- and half-scale circular cylinders and full-, 1/3-, and 1/6-scale airfoil sections. By applying a postulated scaling method, test conditions that should produce scale ice accretions were calculated using the computer code developed for this study. The size and shape of the ice accretions resulting from these test conditions were compared with full-scale results to determine the accuracy of the scaling method. The objectives of the study were met by identifying a scaling method that produces scaled ice accretions over a wide range of test conditions and that can be applied to a variety of icing testing situations.

### **1.3 OUTLINE OF REPORT**

This report begins with a definition of the requirements of icing scaling equations. These requirements are then examined in detail through the development of mathematical models to identify proposed scaling parameters. A review of past icing scaling methods and their respective verifications will also be discussed.

Following the scaling parameter development, the experimental verification procedures and results will be presented. Application of the scaling procedure will be illustrated through the presentation of several scaling examples. Certain limitations identified from the experimental program will also be discussed.

## **2.0 DISCUSSION OF ICING SCALING**

### **2.1 DEFINITION**

Icing scaling is a test procedure used to form similar ice accretions on two geometrically similar objects under different atmospheric and meteorological conditions. "Similar" in this case implies not only identical geometrical shapes but identical surface characteristics, such as the type of ice and roughness. Icing is an accretion process meaning that each layer of ice is formed on the previous layer. This implies that if the ice-accretion process can be started on a clean, model airfoil with surface characteristics similar to a full-scale airfoil, the ice-accretion process will continue similarly and produce scaled ice accretions. This statement forms the major premise of icing scaling and will be applied throughout the development of the scaling parameters. To apply an icing scaling procedure, a set of equations that accurately model the beginning of the icing process must be defined, and parameters that relate the atmospheric conditions of velocity, pressure, and temperature and the meteorological conditions of liquid-water content (LWC), droplet size, and icing time must be identified.

## 2.2 TYPES OF ICING SCALING

The first and most obvious type of icing scaling is that in which the ice accretions are formed on a subscale model similar to those that would be obtained at full-scale. The ability to test subscale geometries would allow smaller test facilities to conduct a wider range of icing tests. Since smaller test facilities are usually less expensive to operate than larger facilities, the cost would be substantially reduced.

A second type of icing scaling, test parameter scaling, is aimed at increasing the simulation capabilities of test facilities by extending the Mach number, altitude, and/or temperature ranges. Icing scaling equations relate the test cell atmospheric and meteorological conditions so that similar ice accretions can be formed. These equations indicate how ground test conditions could be modified to avoid the operational limits of a test facility, yet achieve the appropriate icing condition. For example, a facility may be limited to ambient pressure but have the need to produce an ice accretion that would be formed at an altitude of 10,000 ft. The scaling equations would be applied to determine the test conditions at atmospheric pressure required to simulate the icing that occurs at the altitude flight condition. This type of scaling will allow test facilities to offer a wider range of possible conditions to an aircraft manufacturer to evaluate their flight system.

The applications of both types of scaling would make them very attractive to both the test facility operator and the aircraft manufacturer.

## 2.3 ICING SCALING REQUIREMENTS

The requirements of icing scaling and the individual processes that must be modeled can be identified by examining the ice-accretion process. Ice can form on an object during flight through clouds containing supercooled droplets. These droplets will follow trajectories determined by the forces acting upon them and will either strike or miss the object. The impacting droplets will either freeze in place, run back along the surface and freeze in another location, or run back and be blown off the surface. The shape of the resulting ice accretion will be determined by the distribution of the mass of water striking the airfoil, the locations at which that water freezes, and the type of ice formed. From this elementary description of aircraft icing, the parts of the ice-accretion process that must be considered in an icing scaling analysis can be identified. They are (1) the flow field about the body, (2) the droplet trajectory and impingement characteristics, (3) the total mass of water impinging on the surface, and (4) the thermodynamics of the freezing process. Each of these areas will be evaluated in subsequent sections to identify the scaling parameters used in this study.

### 3.0 IDENTIFICATION OF THE SCALING PARAMETERS

#### 3.1 FLOW FIELD SCALING REQUIREMENTS

First, for the geometrically similar surface conditions required to produce similar ice accretions, it is assumed that the flow field over the bodies, i.e. normalized pressure and temperature distributions, must be similar. This can only be assured if the two bodies have scaled geometries, and the viscous effects are geometrically scaled. The exact duplication of these characteristics, obtained by application of the aerodynamic similitude laws, places stringent restrictions on the test conditions. In general, these requirements are not compatible with the other icing scaling parameters to be discussed in the following sections. An additional assumption must, therefore, be made to relax these requirements.

On an unheated body, an ice accretion will generally form only in the region of droplet impingement. It can therefore be assumed that the normalized pressure and temperature distributions need to be similar only in this region. Except for extreme angles of attack or complex geometries, the droplets generally strike the body in the vicinity of the stagnation point where the boundary layer is relatively thin. While there are Reynolds number effects on the boundary layer even in the stagnation region, the effect on the ice accretion could not be quantified a priori, and therefore, it was assumed that viscous effects are adequately scaled simply by requiring that the bodies are geometrically scaled. The applicability of this assumption was not explicitly evaluated at the beginning of this study because its validity was determined by comparing the full- and subscale ice accretions. In general, the applicability of this assumption for complex test articles and test conditions which may include high angles of attack should be proven either experimentally or analytically prior to conducting the icing test.

The need for similar flow fields indicates that there are velocity limits within which scaling could be accomplished. The velocity distributions around an airfoil will normally be preserved up to the stall as long as the free-stream Reynolds number,  $Re$ , is greater than  $2.0 \times 10^5$  (Ref. 1). This corresponds to a velocity of 31.4 fps for a model airfoil section with a chord of 1.0 ft and a static temperature of  $0^\circ\text{F}$  at an altitude pressure of 10,000 ft. An upper velocity limit is also imposed by the onset of local supersonic flow on the body at the critical Mach number,  $M_c$ . The significant changes in the flow that occur above this upper velocity limit eliminate the possibility of extrapolating results obtained at Mach numbers below  $M_c$  to above  $M_c$ .

From this discussion, the requirements for producing similar flow field characteristics in the impingement region are postulated to be (1) the objects must have scaled geometries, and

(2) the test Mach numbers must be greater than that corresponding to  $Re = 2.0 \times 10^5$  and less than  $M_c$

### 3.2 DROPLET TRAJECTORY SCALING REQUIREMENTS

Not only must the flow about the scaled geometries be similar, but the trajectories of the droplets entrained in this flow must also be similar. A droplet scaling parameter is required to produce geometrically coincident regions of impingement and identical mass distributions on the surfaces of two scaled bodies. The equations of particle motion must be evaluated to identify the parameters that can be used to fulfill these requirements.

The classical particle trajectory equations can be used to calculate droplet trajectories around an object provided that an accurate flow field has been previously calculated. In doing so, it is assumed that the concentration of droplets is small, less than 700 particles/cc, thereby allowing two-phase flow effects and droplet collision and breakup to be neglected. The differential equation describing droplet trajectories normally used in icing studies is

$$m_d \left( \frac{d^2 \vec{X}}{dt^2} \right) = \vec{D} \quad (1)$$

A summary of the simplifications made in the formulation of this equation is given in Ref. 2.

When an appropriate expression for the drag force,  $\vec{D}$ , is substituted and Eq. (1) is nondimensionalized, the following equation results:

$$K \left( \frac{d \vec{U}_d'}{dt'} \right) = \frac{C_D R}{24} \left( \vec{U}_a' - \vec{U}_d' \right) \quad (2)$$

The two nondimensional terms are the inertia parameter,  $K$ , and the droplet Reynolds number,  $R$ , which can be expressed by the following equations:

$$K = \frac{2}{9} \frac{\rho_w r_d^2 U_\infty}{\mu_a c} \quad (3)$$

$$R = \frac{\rho_a d |\vec{U}_a - \vec{U}_d|}{\mu_a} \quad (4)$$

The derivation of Eq. (2) from Eq. (1) is shown in Appendix A.

Equation (2) is used to calculate the droplet trajectory from far upstream to impingement on the body and, if impingement occurs, the total and local collection efficiencies. The total collection efficiency is defined as the ratio of the actual mass of impinging water to the maximum value that would occur if the droplets followed straight-line trajectories. Figure 1 illustrates that this definition can be given in equation form as

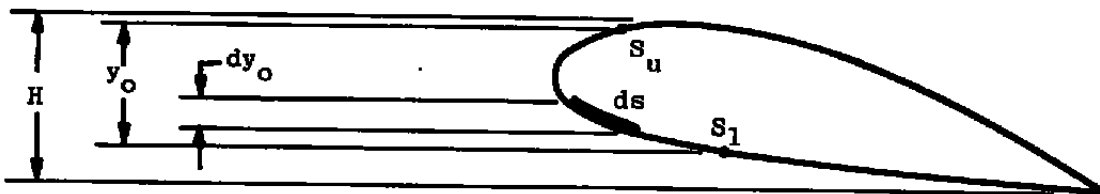
$$E_m = \frac{y_0}{H} \tag{5}$$

where  $y_0$  is the vertical distance between the droplet release points of the upper and lower surface tangent trajectories. The local collection efficiency,  $\beta$ , is also defined in Fig. 1 and can be written in differential form as

$$\beta = \frac{dy_0}{ds} \tag{6}$$

It is related to the total collection by the equation

$$E_m = \frac{1}{H} \int_{S_1}^{S_u} \beta ds \tag{7}$$



- $S_u$  = Upper-Surface Impingement Limit
- $S_1$  = Lower-Surface Impingement Limit
- $H$  = Forward Projection of the Airfoil Height

Total Collection Efficiency

$$E_m = \frac{y_0}{H}$$

Local Collection Efficiency

$$\beta = \frac{dy_0}{ds}$$

$$E_m = \frac{1}{H} \int_{S_1}^{S_u} \beta ds$$

Figure 1. Definition of total and local collection efficiency.

Langmuir and Blodgett (Ref. 3) presented the collection efficiencies (total and local) and the droplet impingement limits about simple geometries as functions of  $K$  and  $R$ , as shown in Figs. 2, 3, and 4. They also developed a term called the modified inertia parameter,  $K_0$ , that can be expressed as

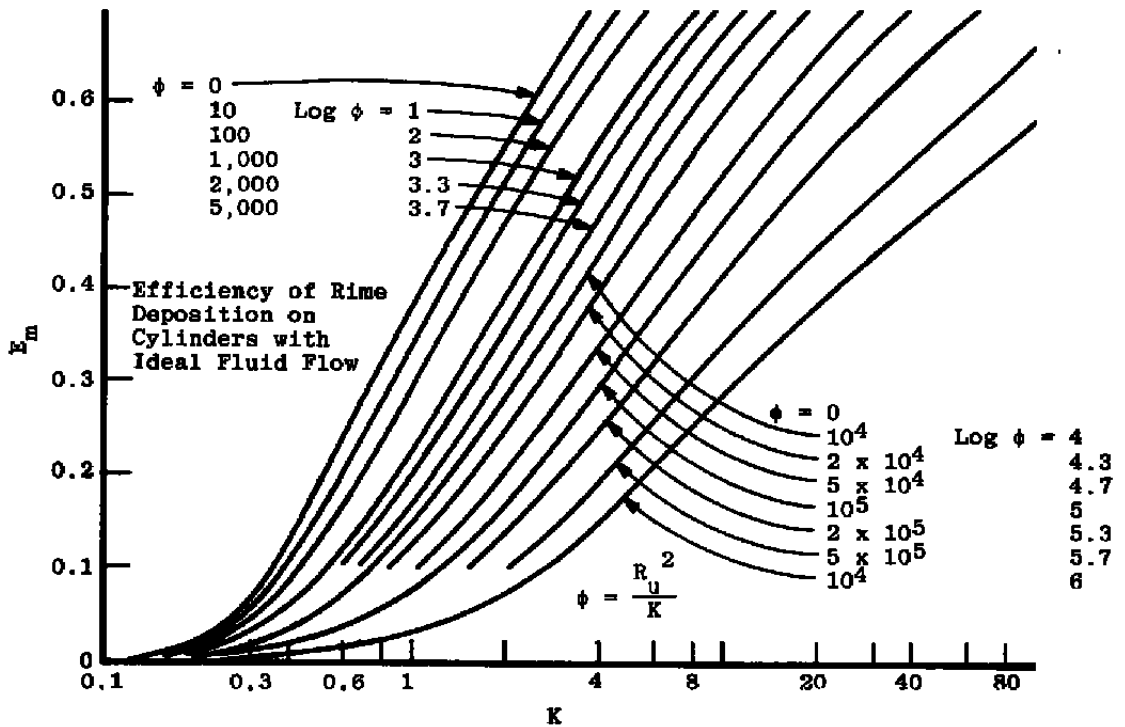


Figure 2. Total collection efficiency versus inertia parameter for a cylinder (Ref. 3).

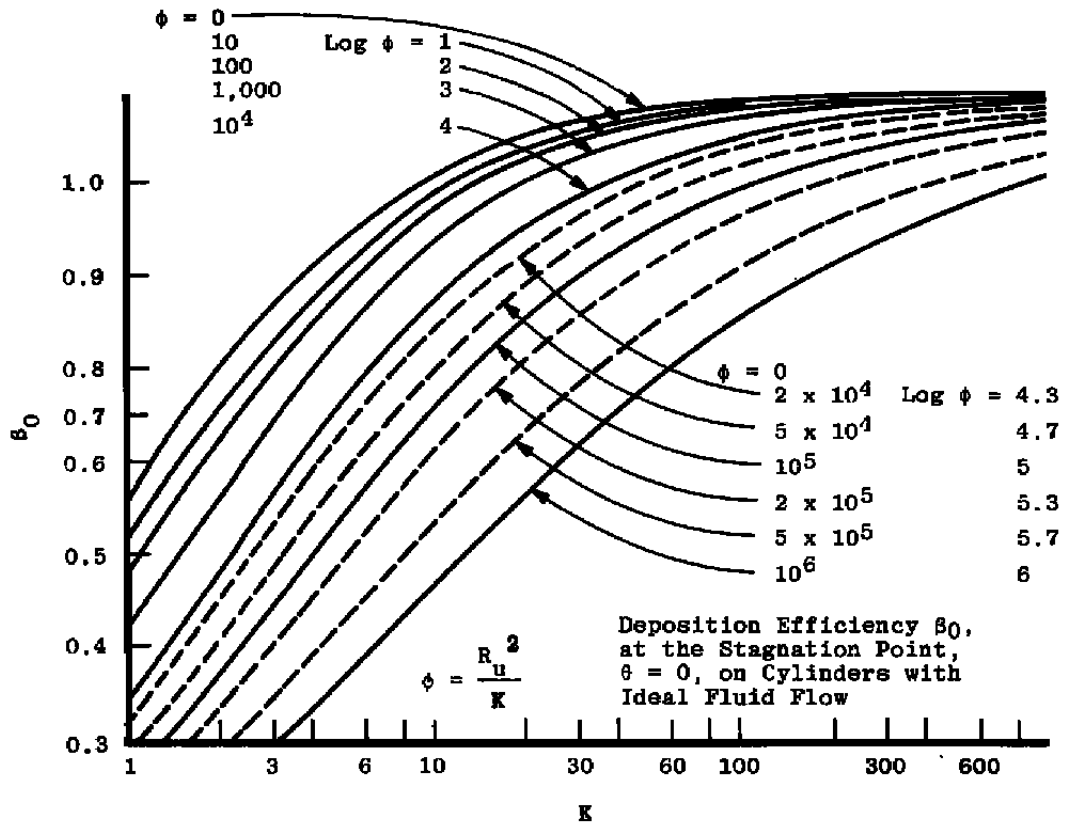


Figure 3. Stagnation-point collection efficiency versus inertia parameter for a cylinder (Ref. 3).



$$K_0 = (\lambda/\lambda_s) K \tag{8}$$

where  $\lambda/\lambda_s$  is defined as the range parameter which is a function of droplet Reynolds number. A further discussion of the droplet range parameter is given in Appendix A. When the calculated impingement characteristics are plotted as functions of  $K_0$ , the family of curves in Figs. 2, 3, and 4 collapse into approximately a single curve. Figure 5, obtained from Ref. 4, shows the plot of  $E_m$  versus  $K_0$  for a cylinder along with the curves for several other geometries.

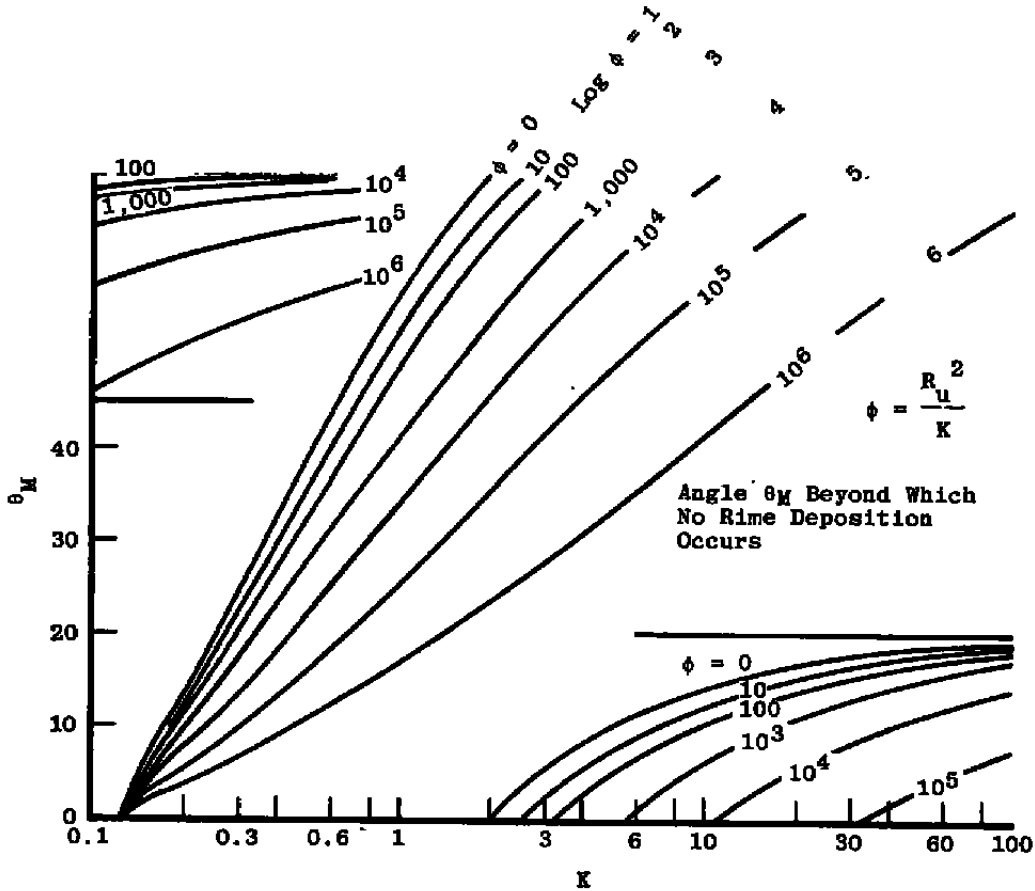


Figure 4. Droplet impingement limit versus inertia parameter for a cylinder (Ref. 3).

Some of the functional dependencies of  $K_0$  are illustrated in Fig. 6 which shows lines of constant  $K_0$  on a plot of droplet size versus velocity. This plot was constructed by calculating  $K_0$  for the specified full-scale condition and then calculating the droplet size required for  $K_0$  to be constant at various model velocities. The curves indicate that for increasing velocities, the subscale droplet size must be reduced so that the effects of droplet inertia on the trajectories are similar. Also, since a subscale model will disturb the flow less than the full-

scale, the droplet diameter for the model condition must also be reduced to maintain the effects of droplet inertia. An increase in static pressure is shown in Fig. 6 to slightly increase the required subscale droplet diameter. In the range of static temperatures encountered in most icing analysis, the effect of temperature on  $K_0$  and the resulting subscale droplet diameter is negligible.

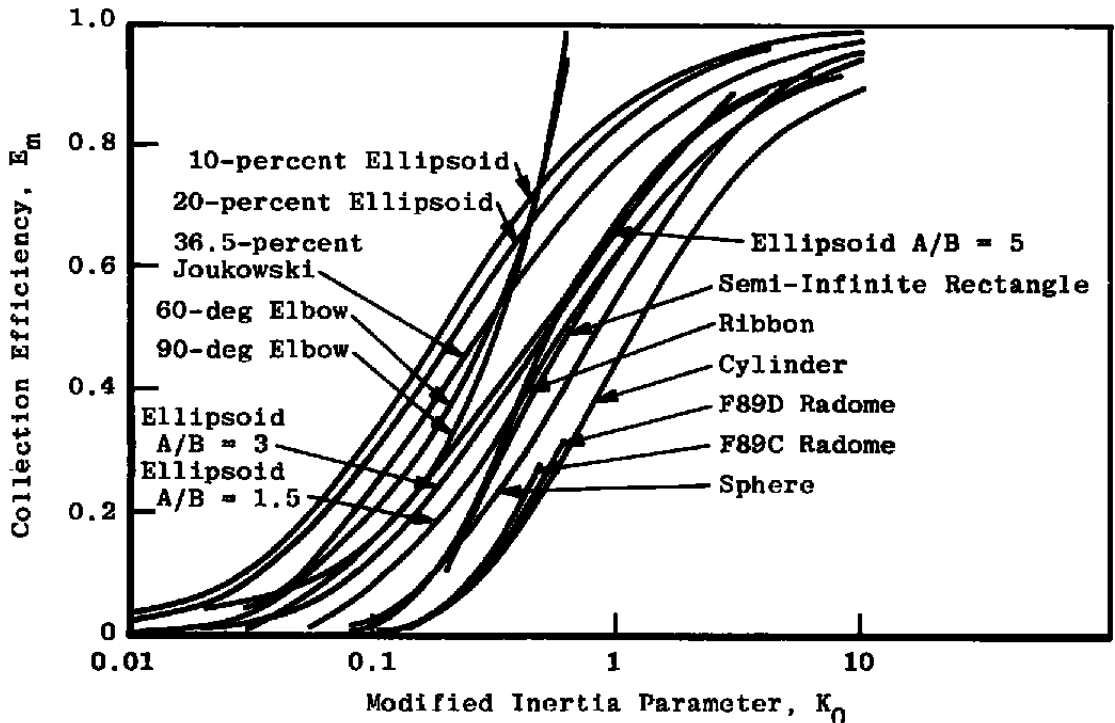


Figure 5. Total collection efficiency versus modified inertia parameter for various geometries (Ref. 4).

To verify  $K_0$  as a droplet scaling parameter, it must be shown that (1) the trajectory equations from which  $K_0$  is derived can be used to predict experimentally obtained impingement characteristics, and (2) these characteristics are indeed scaled for conditions with constant  $K_0$ . The first requirement has been evaluated by previous droplet trajectory studies conducted by Bragg (Ref. 2) and Frost (Ref. 5). Good agreement with experimental data was obtained in both studies. Bragg also satisfied the second requirement by showing examples of similar droplet impingement characteristics obtained at conditions with constant values of  $K_0$ .

In a test facility, as in nature, an icing cloud is composed of a distribution of droplet diameters. To avoid calculating the value of  $K_0$  and local collection efficiency for each of the droplet sizes, the icing cloud is characterized by a single mass median droplet diameter. The

Full-Scale Condition:  $K_0 = 0.55$

2.0-in.-diam Cylinder

$P_S = 12.2$  psia

$T_S = 20^\circ\text{F}$

$\bar{d}_m = 20$   $\mu\text{m}$

$U_\infty = 250$  fps

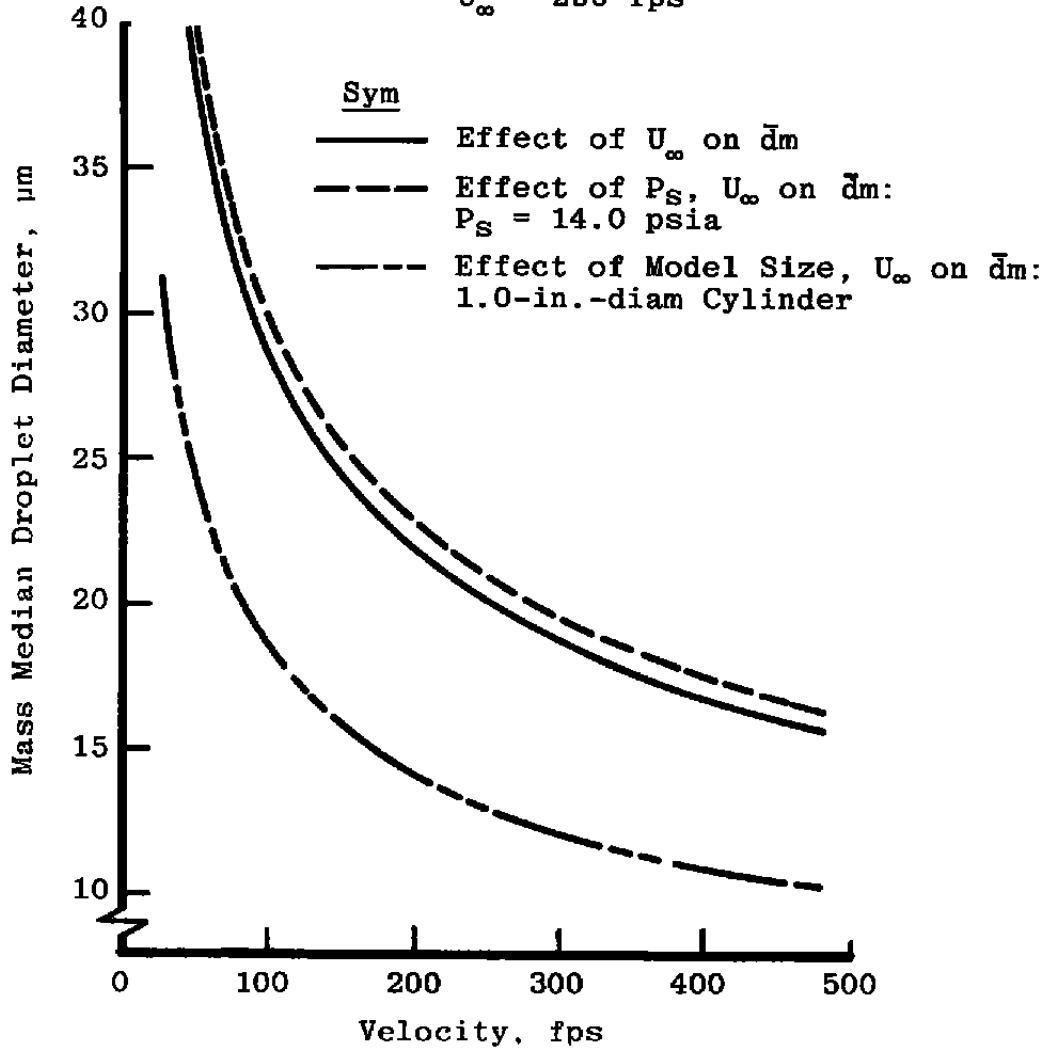


**Figure 6. Effect of velocity, static pressure, and model size on the mass median droplet diameter for a constant value of modified inertia parameter,  $K_0$ .**

mass median droplet diameter is defined as that diameter below which half of the total mass of liquid water is contained. The validity of this characterization has been demonstrated by Chang (Ref. 6). Figure 7 shows a comparison of the local collection efficiency calculated for a multidispersed droplet distribution (Langmuir D) and for the mass median droplet diameter characterizing that distribution. Note that excellent comparison with experiment is achieved using either the multidispersed or monodispersed clouds in the stagnation region but that the entire droplet distribution must be included to accurately evaluate the characteristics near the impingement limits. As will be discussed in Section 3.4, the agreement in the stagnation region is sufficient to verify the use of the mass median droplet diameter to characterize the icing cloud when applied to scaling studies. All further references to droplet diameter contained in the text imply the mass median droplet diameter of the icing cloud unless otherwise specified.

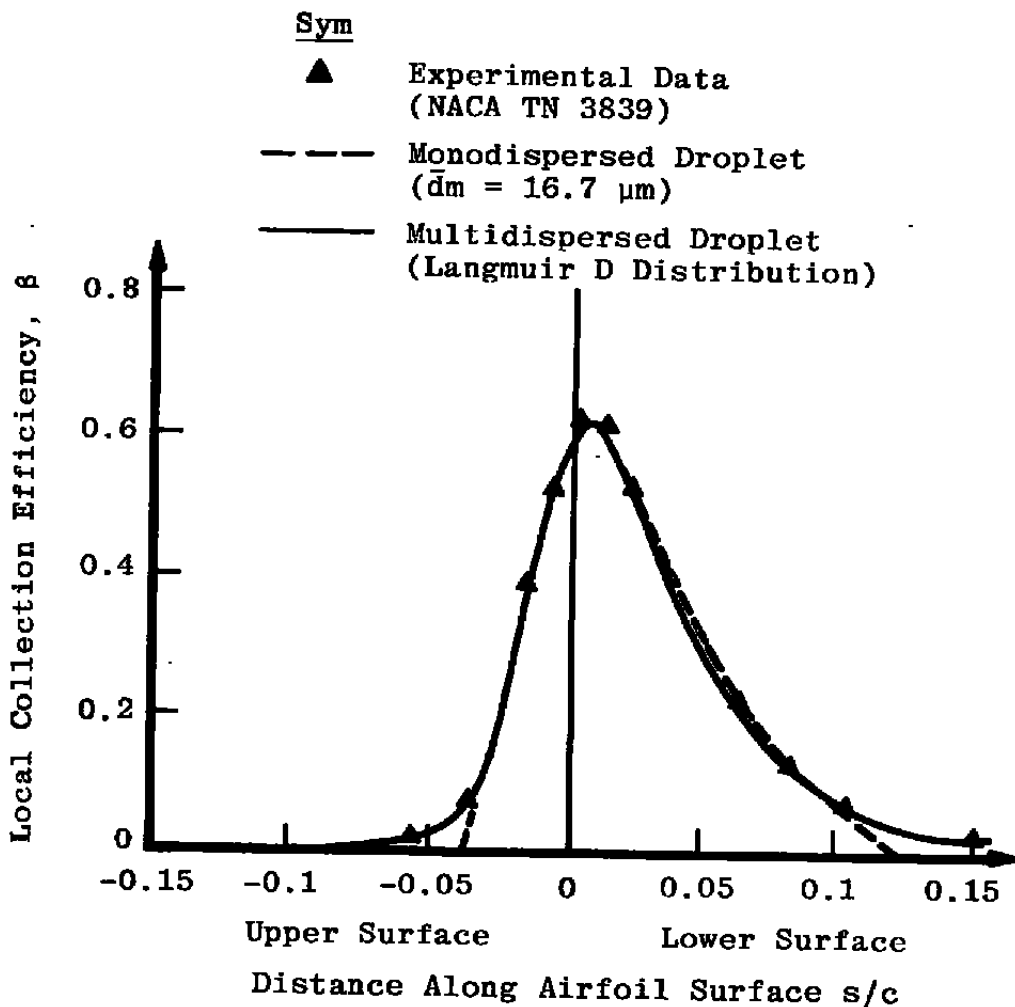


**Figure 7. Comparison of local collection efficiency calculations using monodispersed and multidispersed droplet distributions (Ref. 6).**

The above results show that  $K_0$ , based on the mass median droplet diameter, satisfies the requirements of a droplet scaling parameter. The scaling equation for droplet trajectories can, therefore, be written as follows:

$$(K_0)_{\text{model}} = (K_0)_{\text{full-scale}} \quad (9)$$

### 3.3 TOTAL WATER-CATCH SCALING REQUIREMENTS

Droplet trajectory scaling has assured that the normalized distribution of impinging mass on the surface of the body is similar. For ice accretions formed on two geometrically scaled objects to be similar, the total mass of impinging water per unit area should be scaled, i.e.

$$(m_w^*)_{\text{model}} = k (m_w^*)_{\text{full-scale}} \quad (10)$$

where  $k$  is the model scale factor given by the following ratio:

$$k = \frac{c_m}{c_f} \quad (11)$$

The full- and subscale characteristic lengths,  $c_m$  and  $c_f$ , respectively, can be any scaled dimension but were taken to be the airfoil chord or cylinder diameter in this study. Substituting Eq. (11) into Eq. (10), the following equation results:

$$\left( \frac{m_w^*}{c} \right)_{\text{model}} = \left( \frac{m_w^*}{c} \right)_{\text{full-scale}} \quad (12)$$

The total mass of water impinging at a specific location on the surface in a time interval,  $\tau$ , is given by the following equation:

$$m_w^* = \text{LWC} (U_\infty) \beta \tau \quad (13)$$

Substituting Eq. (13) into Eq. (12) results in a relationship that will scale the total mass of water per unit area impinging at each point on geometrically scaled objects,

$$\left[ \frac{\text{LWC} (U_\infty) \beta \tau}{c} \right]_{\text{model}} = \left[ \frac{\text{LWC} (U_\infty) \beta \tau}{c} \right]_{\text{full-scale}} \quad (14)$$

Since the modified inertia parameter scaling has ensured that the local collection efficiencies at each location on the surface are the same,  $\beta$  can be cancelled from both sides of Eq. (14) to yield the following expression:

$$\left[ \frac{\text{LWC} (U_\infty) \tau}{c} \right]_{\text{model}} = \left[ \frac{\text{LWC} (U_\infty) \tau}{c} \right]_{\text{full-scale}} \quad (15)$$

Note that Eq. (15) is now independent of the location,  $s$ , on the surface.

Past icing analyses by various authors have related the terms of Eq. (15) to an ice thickness by dividing by the ice density. The resulting term, called the accumulation parameter, can therefore be expressed as

$$A_c = \frac{\text{LWC} (U_\infty) \tau}{\rho_i c} \quad (16)$$

Since the type of ice formed on a subscale accretion is to be the same as that formed on the full-scale, the ice densities must be identical. Equation (15) can therefore be rewritten in terms of the accumulation parameter as

$$(A_c)_{\text{model}} = (A_c)_{\text{full-scale}} \quad (17)$$

Figure 8 shows the functional dependencies of the terms in the accumulation parameter. The plot shows that for a constant LWC, as the velocity is increased, the icing time must decrease so that the total mass of impinging water remains scaled. Reducing the model size at a constant velocity is also seen to reduce the icing time so that a scaled mass of water is deposited.

In summary, this analysis has indicated that, if the accumulation parameter,  $A_c$ , is held constant, the total mass of water per unit area impinging on the surface of full- and subscale geometries will be scaled. The scaling equation expressing this requirement is given by Eq. (17).

### 3.4 THERMODYNAMIC SCALING REQUIREMENTS

Thermodynamic scaling, or energy equation scaling as it is commonly called, is required so that the type, surface characteristics, and density of the ice accretion is similar between the full- and subscale test articles. To formulate the mathematical expression required to define the thermodynamic scaling parameters, it is necessary to develop a physical model of the ice-accretion process.

The assumption made in the discussion of the flow field requirements was that if the geometries are scaled, the normalized pressure and temperature distributions in the region of droplet impingement will be similar. Also, the droplet impingement parameter,  $K_0$ , has been

shown in Refs. 2 and 5 to accurately duplicate the distribution of mass on the surface for two scaled conditions. Since these parameters serve as the input to the thermodynamic analysis, the distribution of the thermodynamic characteristics, for example, the normalized surface temperature distribution, should also be similar to that of the full-scale. To produce identical thermodynamic characteristics in the impingement region given similar input distributions, it is assumed to be only necessary to match the characteristics at one point. The stagnation point is chosen because data exist for the heat-transfer coefficient and local collection efficiency in that region for a variety of body geometries. This assumption could not be evaluated a priori because sufficiently accurate experimental, and analytical data does not exist at this time. Therefore, as in the analysis of the flow field, the validity of the assumption was determined by comparing the full- and subscale ice accretions. All values of the thermodynamic parameters reported herein are evaluated at the stagnation point. Recall that Fig. 7 showed that the mass median droplet diameter could be used to characterize the droplet distribution in an icing cloud in the vicinity of the stagnation point.

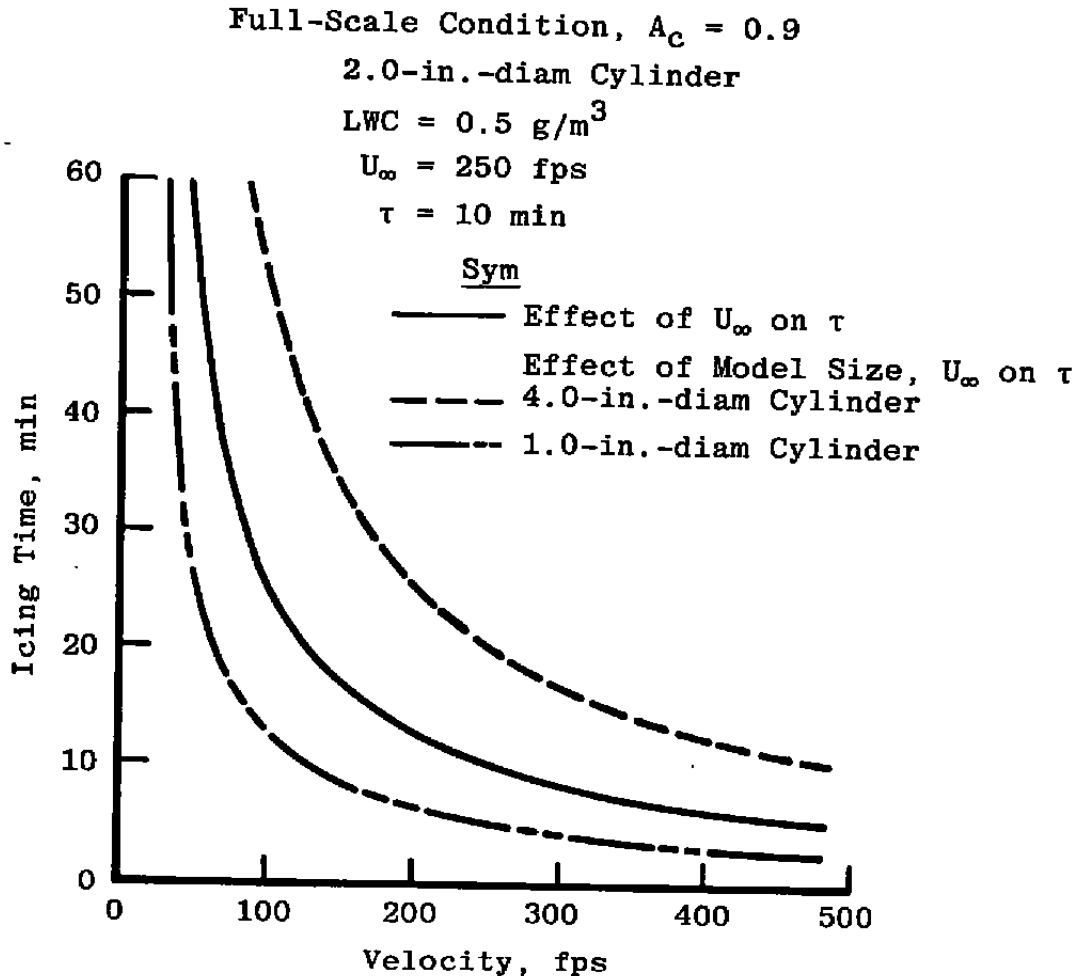


Figure 8. Effect of velocity and model size on the icing time for a constant value of accumulation parameter,  $A_c$ .

The physics of stagnation-line icing has been observed at NASA Lewis Research Center using microscopic observation techniques (Ref. 7). The observations have shown that when droplets initially strike an ice-free surface, they coalesce into larger drops and then run back along the surface. By applying the premise in Section 2.1 which states that if the ice accretions can be started under similar conditions, they will grow similarly, the observed initial phase of the ice-accretion process is all that has to be modeled, and the more complicated problem of modeling the formation of ice on a previously deposited ice layer is avoided. A thermodynamic equation of the initial phase of the stagnation-line process can be formulated from the above observations and used to define the scaling parameters to be used in this study.

### 3.4.1 Icing Thermodynamic Model

The thermodynamic analysis of an icing surface was first presented by Tribus (Ref. 8) and was used to calculate the heating requirements for icing protection and proposed LWC measurement systems. Messinger (Ref. 9) developed the model further to include an analysis of the temperature of an unheated surface in icing conditions in three free-stream temperature regimes, i.e. less than 32°F, equal to 32°F, and above 32°F, and the concept of the freezing fraction,  $n$ , to be discussed later. These early formulations have been used in various icing applications over the years. Modifications to these early models have consisted mainly of adding the effects of compressibility in the flow about an airfoil. The model for stagnation-line icing used in this study is slightly different from that of previous work because both the mass and energy balance are addressed. The form of the energy equation used in this study can be expressed as follows:

$$\begin{aligned}
 W_w \left[ c_{p_{w,s}} (T_s - 32) + \frac{U_\infty^2}{2g_c J} \right] &= \dot{W}_e L_v \\
 + (1 - n) W_w \left[ c_{p_{w,sur}} (T_{sur} - 32) \right] & \\
 + n W_w \left[ c_{p_{i,sur}} (T_{sur} - 32) - L_f \right] + h_c \left[ T_{sur} - T_s - \frac{U_\infty^2}{2g_c J c_{p_a}} \right] & \quad (18)
 \end{aligned}$$

The complete derivation of Eq. (18) is included in Appendix B.

Dividing Eq. (18) to the convective heat-transfer coefficient,  $h_c$ , results in the following form of the energy equation:

$$\begin{aligned}
 -b\phi &= \theta + (1 - n) \frac{W_w}{h_c} [c_{p_{w,sur}} (T_{sur} - 32)] \\
 + n \frac{W_w}{h_c} [c_{p_{i,sur}} (T_{sur} - 32) - L_f] & \quad (19)
 \end{aligned}$$



where

$$b = \frac{W_w c_{pws}}{h_c} \quad (20)$$

$$\phi = 32 - T_s - \frac{U_\infty^2}{2g_c Jc_{pw,s}} \quad (21)$$

$$\theta = \left[ T_{sur} - T_s - \frac{U_\infty^2}{2g_c Jc_{pR}} \right] + \frac{W_e}{h_c} L_v \quad (22)$$

The above terms will be discussed in Section 3.4.3. Before applying the above equation to an icing analysis it was necessary to evaluate experimentally the range of applicability of the stagnation-line thermal model.

### 3.4.2 Verification of the Thermal Model

The experimental verification of the thermal model for stagnation-line icing is difficult and has been limited to comparison between measured and calculated surface temperatures, icing onset temperatures, and stagnation-line ice growth rates. Since the experimental determination of the icing onset temperature is somewhat subjective, and the stagnation-line growth rate is dependent on precisely knowing the ice density, the comparison of surface temperatures is considered the most accurate means of verifying the thermal model. Recent work in this area has been done by Fergus (Ref. 10), who found that comparisons with experiment were fairly accurate when a correction factor was applied to the evaporative energy flux term. Figure 9 shows that the current model compares well with Fergus' corrected model without the need for the evaporation term correction and that both models predict the surface temperature near 32°F to within 1.5°F. Given the errors in measuring the temperature of a surface undergoing icing, these results provide a measure of confidence in the thermal model but definitely do not provide the desired verification. It will therefore be assumed that the accuracy of the thermal model is sufficient for application in a scaling analysis and that the validity of this assumption will be determined by comparing the full- and subscale ice accretions.

### 3.4.3 Thermodynamic Scaling Parameters

Several thermodynamic scaling parameters have been proposed in past icing scaling studies but, in general, without discussion of their physical significance. The following sections will define the scaling parameters used in this study and discuss their significance through the presentation of ice-accretion examples and figures.

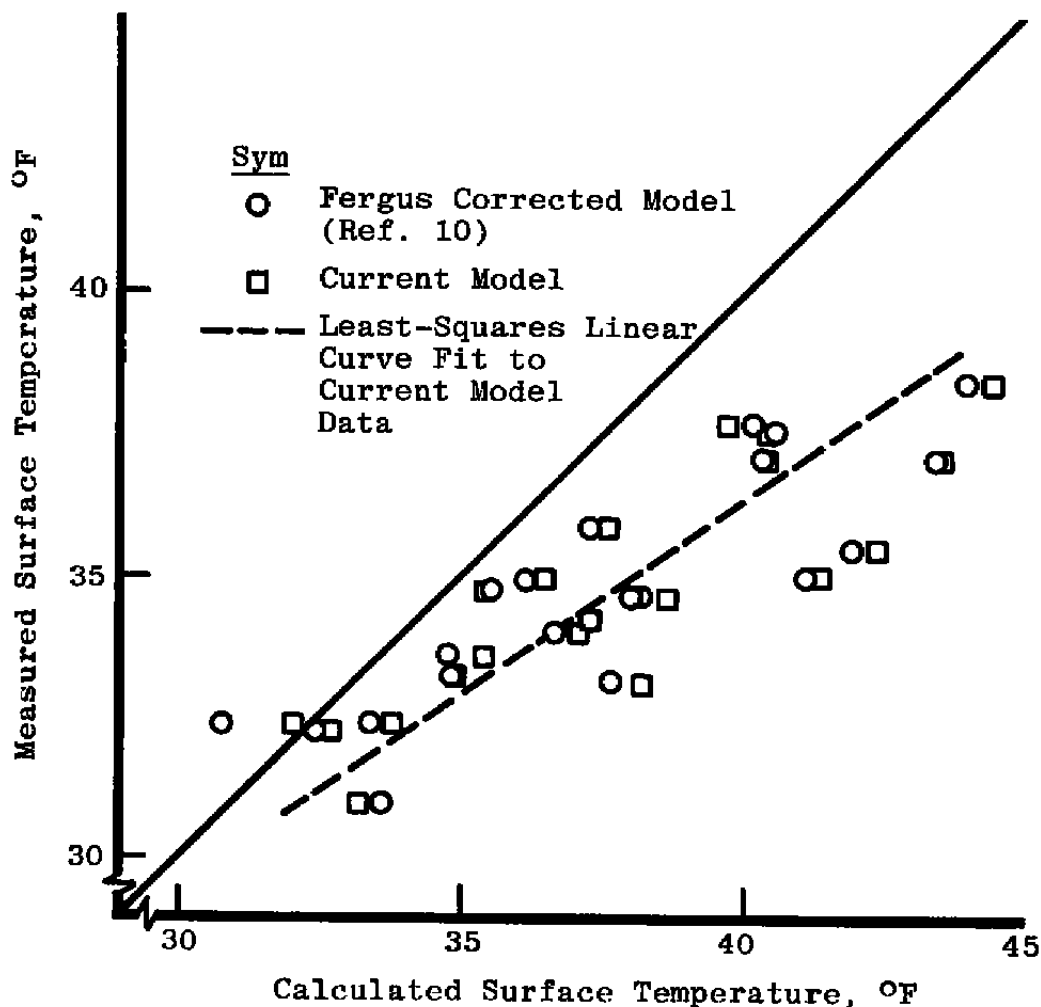


Figure 9. Comparison of measured and calculated surface temperatures in incipient icing conditions.

### 3.4.3.1 Freezing Fraction

The freezing fraction,  $n$ , was defined by Messinger as being the fraction of impinging liquid which freezes in the region of impingement. For colder icing conditions, the droplets tend to freeze immediately on impact resulting in a rime ice accretion, as shown in Fig. 10a. Rime ice is milky white, opaque, and characterized by a calculated stagnation-point freezing fraction equal to 1.0. Since the droplets freeze on impact, the accretion is fairly smooth and aerodynamically shaped.

Freezing fractions close to zero characterize glaze ice accretions which are composed of clear ice and, in general, have well-defined horns, as shown in Fig. 10b. These horns form

initially because of liquid water running along the surface away from the stagnation point and then freezing at some point further aft where the convective heat transfer is sufficiently increased to remove the latent heat of fusion. The roughness of this accretion then enhances the convective heat transfer, causing the horns to continue to grow. As the horns grow, the collection efficiency in this region also increases, contributing further to the growth of the horns.

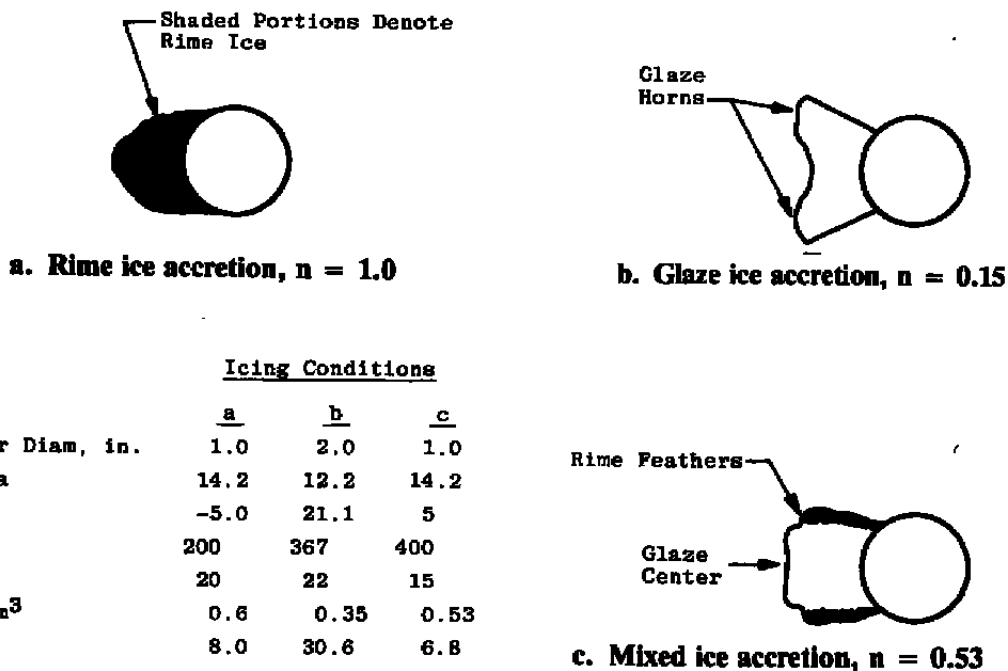


**Figure 10. Examples of ice accretions formed at various values of stagnation-point freezing fraction.**

Ice accretions with calculated freezing fractions between approximately 0.3 and 1.0 will normally have some of the characteristics of both rime and glaze ice and are referred to as mixed ice accretions. Fig. 10c shows that the center portion will be predominantly glaze but will be surrounded by rime accretions. The size of the glaze center will decrease as the freezing fraction nears 1.0.

The predominant functional dependencies of the freezing fraction are shown by the lines of constant freezing fraction in Fig. 11. As the LWC is increased, the energy added to the surface by the droplets is also increased. The velocity must, therefore, be reduced to decrease the aerodynamic heating and kinetic energy of the droplets to allow the same fraction

of the impinging water to freeze. An increase in the static temperature at a constant velocity requires that the LWC be reduced, again to maintain the proper freezing fraction. A slight variation of LWC with static pressure is also shown.

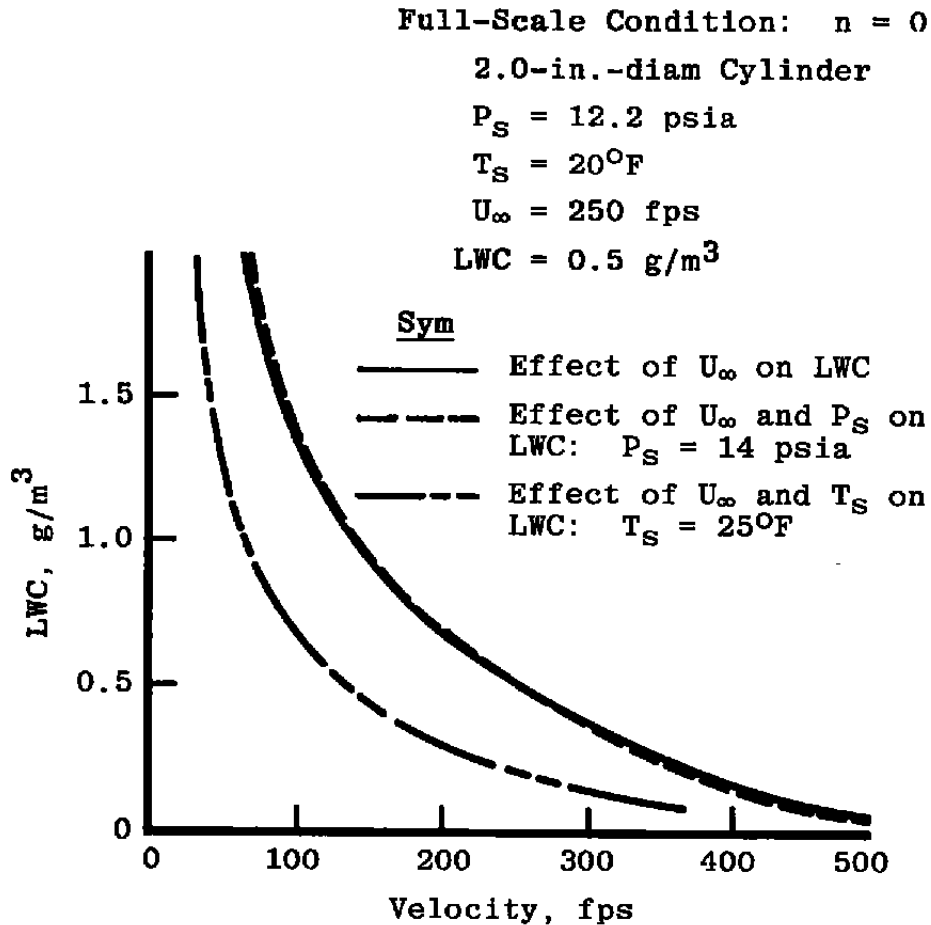


**Figure 11. Effect of velocity, static pressure, and static temperature on LWC for a constant value of freezing fraction,  $n$ .**

The above discussion indicates that the freezing fraction does have a distinct physical significance in the formation of ice accretions. It has been postulated in previous scaling studies that the freezing fraction must be held constant to produce similar ice accretions and has, therefore, been included in this study. A third scaling equation can, therefore, be written as follows:

$$(n)_{\text{model}} = (n)_{\text{full-scale}} \quad (23)$$

3.4.3.2 Relative Heat Factor

The relative heat factor,  $b$ , was defined by Tribus (Ref. 8) as being a measure of the ratio of the sensible heat-absorbing capacity of the impinging water per unit of surface area to the unit convective heat-dissipating capacity of the same surface. It was previously defined in Eq. (20), rewritten here as

$$b = \frac{LWC (U_\infty) \beta c_{p_{w,s}}}{h_c} \tag{24}$$

where  $c_{p_{w,s}}$  is the specific heat of water. Note that the relative heat factor is nondimensional, and since it contains the local convective heat-transfer coefficient,  $h_c$ , and local collection efficiency,  $\beta$ , is dependent upon geometry.

Figure 12 shows lines of constant  $b$  for the specified conditions. As indicated by Eq. (24), as the velocity increases, the LWC must decrease. The figure also shows that  $b$  is relatively

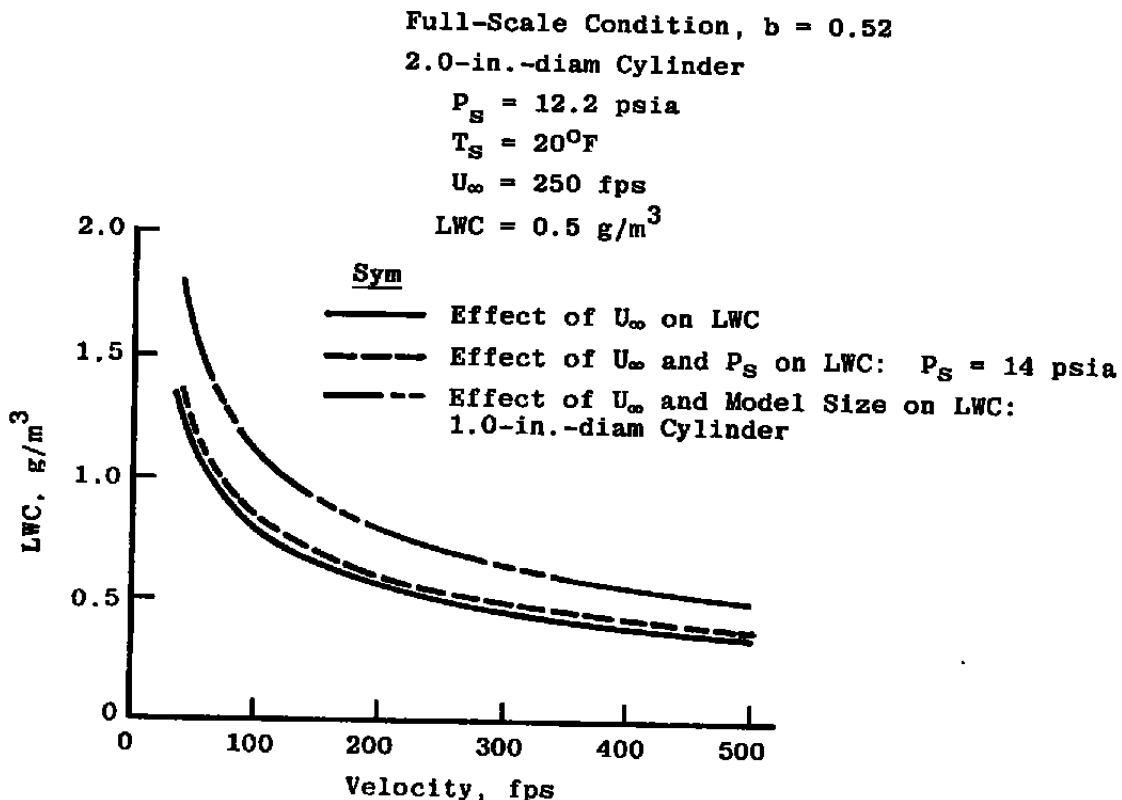


Figure 12. Effect of velocity, static pressure, and model size on LWC for a constant value of relative heat factor,  $b$ .

insensitive to static pressure which enters only through the convective heat transfer and local collection efficiency. A decrease in the size of the geometry will increase the convective heat-transfer coefficient requiring that the LWC also be increased to maintain a constant value of  $b$ . The effect of static temperature on the LWC required for the relative heat factor to be constant is negligible, at least in the range of temperatures applicable to icing studies.

It has been postulated in previous icing studies, Refs. 11, 12, and 13 that the relative heat factor must be held constant to produce scaled ice accretions. A fourth scaling equation to be evaluated in this study can, therefore, be expressed as follows:

$$(b)_{\text{model}} = (b)_{\text{full-scale}} \quad (25)$$

### 3.4.3.3 Droplet and Air Energy Transfer Driving Potentials

Equation (19) identified two additional parameters,  $\phi$  and  $\theta$ , given by Eqs. (21) and (22), respectively, which are rewritten below

$$\phi = 32 - T_s - \frac{U_\infty^2}{2g_c Jc_{p_{w,s}}} \quad (26)$$

$$\theta = \left[ T_{\text{sur}} - T_s - \frac{U_\infty^2}{2g_c Jc_{p_a}} \right] + \frac{W_e}{h_c} L_v \quad (27)$$

Equations 26 and 27 show that  $\phi$  and  $\theta$  have the units of temperature and contain terms relating to the droplet and air energy transfer, respectively. Insight into their significance can be gained by examining the general equation for the convective heat flux given as

$$q_c = h_c \Delta T \quad (28)$$

In this equation,  $\Delta T$  is the temperature difference that acts as the driving potential for this mode of heat transfer. Since  $\phi$  and  $\theta$  also have units of temperature and contain terms relating to the energy transfer caused by the droplets and the airflow, they can, by analogy, be considered to be droplet and air energy transfer driving potentials, respectively.

Figure 13 shows the relationship between the static temperature and the velocity that is indicated by Eq. (26). This curve was constructed so that the value of  $\phi$  was constant. It is interesting to note that the total or stagnation enthalpy,  $i_T$ , is also constant along this line. Therefore,  $\phi$  is a measure of the total enthalpy of the impinging water.

Equation (27) shows that  $\theta$  is a function of static pressure, temperature, and velocity. Lines of constant  $\theta$  for various temperatures are shown in Fig. 14. Note that a 5.0-deg increase in static temperature causes the static pressure to be significantly reduced. This indicates that if  $\theta$  is held constant, small changes in the static temperature can require significant changes in static pressure. Also, note that static pressures above standard sea-level pressure of 14.7 psia can be calculated.

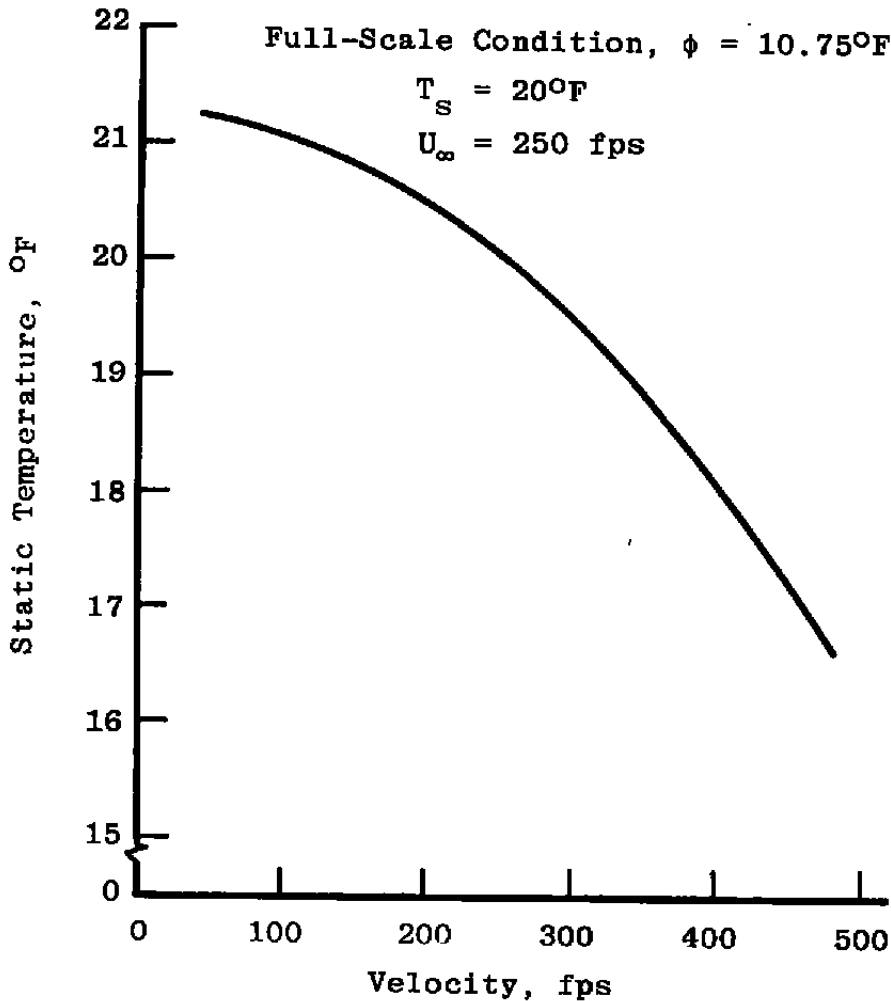


Figure 13. Effect of velocity on static temperature for a constant value of droplet energy potential,  $\phi$ .

In summary, the following scaling equations will be evaluated in the experimental portion of this study:

$$(K_0)_{\text{model}} = (K_0)_{\text{full-scale}}$$

$$(A_c)_{\text{model}} = (A_c)_{\text{full-scale}}$$

$$(n)_{\text{model}} = (n)_{\text{full-scale}}$$

$$(b)_{\text{model}} = (b)_{\text{full-scale}}$$

$$(\phi)_{\text{model}} = (\phi)_{\text{full-scale}}$$

$$(\theta)_{\text{model}} = (\theta)_{\text{full-scale}}$$

Full-Scale Condition,  $\theta = 14.40^\circ\text{F}$

$$T_s = 20^\circ\text{F}$$

$$P_s = 12.2 \text{ psia}$$

$$U_\infty = 250 \text{ fps}$$

———— Effect of  $U_\infty$  on  $P_s$

----- Effect of  $U_\infty$  and  $T_s$  on  $P_s$ :  
 $T_s = 25^\circ\text{F}$

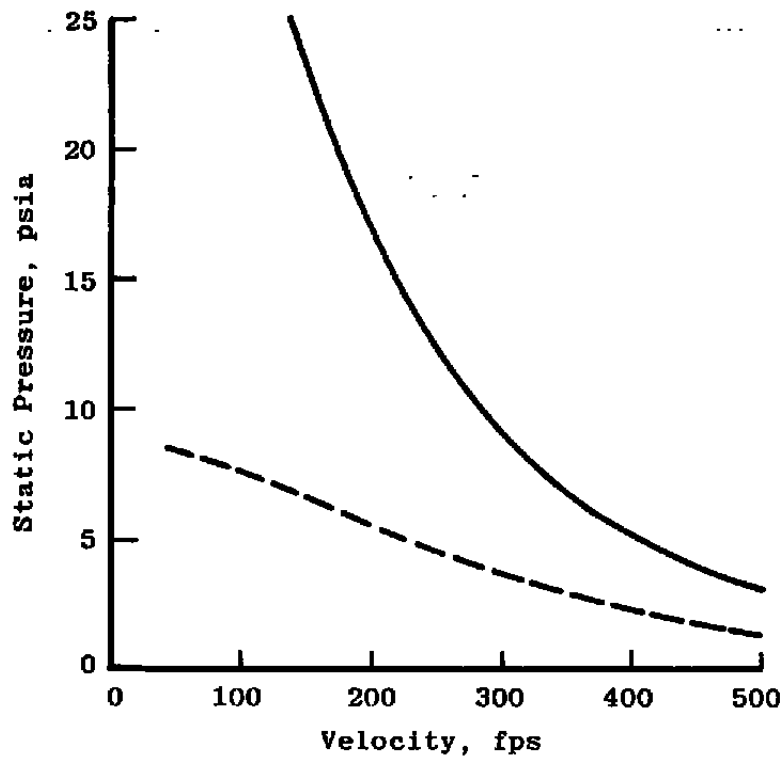


Figure 14. Effect of velocity and static temperature on static pressure for a constant value of air energy potential,  $\theta$ .



## 4.0 SCALING METHODS INVESTIGATED

### 4.1 PAST SCALING INVESTIGATIONS

In Section 3.0, a proposed set of icing scaling parameters were presented. Various combinations of the parameters have been postulated to produce similar ice accretions in previous studies. Table 1 shows five of the most well-known formulations of scaling equations and the combination of parameters proposed by each. The equations proposed by Armand (Ref. 13) are similar to those derived in this report and, of the studies listed, was the only one to provide experimental verification. However, the limitations of the test facility used in that study did not allow adequate verification of the parameters, especially those satisfying thermal similitude. Therefore, experimental efforts were begun at the Arnold Engineering Development Center (AEDC) and NASA Lewis Research Center with the purpose of comparing various scaling methods and experimentally verifying a set of scaling equations. The remainder of this section will describe the scaling methods evaluated at the AEDC.

Table 1. Summary of Past Scaling Investigations

Scaling Analysis	Scaling Parameters					
	$K_0$	$A_c$	$n$	$b$	$\phi$	$\theta$
Douglas Aircraft Co., 1954 (Ref. 14)	X	X				
Lockheed Aircraft Corp., 1955 (Ref. 11)	X	X	X	X		
Boeing Airplane Co., 1962 (Ref. 15)	X	X				
British Aircraft Corp., 1967 (Ref. 12)	X	X	X	X		
ONERA Modane Centre, France, 1977 (Ref. 13)	X	X	X	X	X	X

### 4.2 IDENTIFICATION OF THE SCALING METHODS

The purpose of the experimental portion of this study was to determine which of the proposed scaling parameters are necessary and sufficient to produce scaled ice shapes. All scaling studies agree that the droplets must impinge on the surface in geometrically similar

locations and that scaled masses of water per unit area must impinge on the surface to produce scaled ice shapes. Therefore,  $K_0$  and  $A_c$  are generally accepted as the droplet and accumulation scaling parameters, respectively. The studies differ on which, if any, of the energy equation scaling parameters are necessary to produce similar ice accretions. Four scaling methods were selected for evaluation in this study and are described below.

#### **4.2.1 Method 1: $K_0$ and $A_c$ Constant**

This method is the simplest to apply because only  $K_0$  and  $A_c$  are held constant. The static pressure and temperature are held constant, and the LWC, icing time, and velocity can be varied as long as  $A_c$  remains constant. The droplet diameter is chosen so that  $K_0$  is constant.

#### **4.2.2 Method 2: $K_0$ , $A_c$ , and $n$ Constant**

Energy equation scaling is applied in this method by requiring that the freezing fraction be held constant in addition to the parameters in Method 1. The static pressure, velocity, and LWC of the model condition are specified, and the static temperature is then calculated so that  $n$  is held constant.

#### **4.2.3 Method 3: $K_0$ , $A_c$ , $n$ , and $b$ Constant**

In this method, the relative heat factor is held constant in addition to those in Method 2. The velocity and static pressure of the model condition can be specified, and the LWC is calculated so that  $b$  is held constant. The static temperature of the model icing condition is again calculated from the energy equation so that  $n$  is held constant. The value of  $A_c$  is maintained by selecting the proper icing time.

#### **4.2.4 Method 4: $K_0$ , $A_c$ , $n$ , $\phi$ , and $\theta$ Constant**

The air and droplet energy transfer driving potential terms are held constant in this method along with those in Method 2. It is the most restrictive of the four because only the model scale and velocity can be specified. All other test parameters are determined from the equations. A summary of the methods and the requirements of each are given in Table 2.

### **4.3 SOLUTION OF THE SCALING EQUATIONS**

Many of the past scaling investigations solved the scaling equations graphically. The complexity of the scaling equations contained in the above methods make them suited for solution by computer. An icing similitude code, SIMICE, was written for the Air Force by Professor W. W. Bowden of Rose-Hulman Institute of Technology in 1981 under contract

with the AEDC. While the form of the code was not applicable to this study, it did contain subroutines that calculated many of the physical constants that are required for the solution of Eq. (18). The code was modified so that each of the above scaling methods could be solved individually and was used to calculate test conditions in the experimental portion of this study.

**Table 2. Summary of the Scaling Methods Investigated at the AEDC**

Method	Parameters Held Constant				
	Modified Inertia Parameter	Accumulation Parameter	Freezing Fraction	Relative Heat Factor	Energy Terms
1	X	X			
2	X	X	X		
3	X	X	X	X	
4	X	X	X		X

## 5.0 EXPERIMENTAL VERIFICATION

As previously stated, most of the past scaling investigations did not present experimental data verifying the proposed scaling method. When experimental data were presented, it was not sufficient to identify the limitations of the method so that the data could be used with confidence in icing tests. The purpose of the experimental study discussed below was to investigate icing scaling to provide a more complete understanding of the application of the various scaling methods and to determine which, if any, of the proposed methods produced scaled ice accretions. The following section discusses the procedures used to select test conditions and to measure and compare the resulting ice accretions.

### 5.1 SCALING TEST PROCEDURES

The experimental study was begun by identifying and testing a set of icing conditions on a full-scale geometry. The profiles of the ice accretions obtained from these full-scale test conditions were measured using calipers and chilled carpenter's profile gauges. When the ice accretion was large enough to allow removal from the surface, it was removed and dipped in beeswax, producing a mold from which a plaster casting was made. The casting provided another record of the ice-accretion profile and of the surface roughness characteristics.

The icing similitude computer code developed for this study, SIMICE, was then used to calculate the test conditions for the subscale geometry. Conditions were also calculated for the full-scale geometry to evaluate test parameter scaling discussed in Section 2.2. The calculated test conditions were then run, and the ice-accretion characteristics were again measured and recorded.

Small differences between the desired test condition and the actual condition run are present in practically all types of testing. The effect of these differences on the values of the scaling parameters can be calculated, but the effect of differences in the scaling parameters on the similarity of the ice accretions was not known prior to the tests. Therefore, all test conditions were reevaluated after the test using SIMICE to determine values of the scaling parameters for the actual condition run. The relative similarity of the full- and subscale ice accretions was then evaluated by comparing the profiles of the accretions and the size and locations of the glaze horns, or, in the case of mixed ice accretions, the glaze and rime portions. When necessary, the profiles were drawn to the same scale to facilitate more accurate comparisons. Since the drag increase caused by the shape and surface roughness of the ice accretions could not be measured in the test cell, comparison of the surface characteristics was limited to comparison of the experimental observations and plaster casts of the ice accretion.

The scaling methods to be evaluated can only be expected to scale the dimensions of the ice accretions to within the repeatability of two accretions formed at identical conditions. The repeatability of the dimensions is dependent on the precision of the test facility and the measurement technique. Figure 15 shows the repeatability of two glaze accretions formed at identical atmospheric and meteorological conditions to be on the order of 10 percent. Therefore, a scaling method may be considered successful if the type of ice formed is similar in appearance and the dimensions are scaled to within approximately 10 percent.

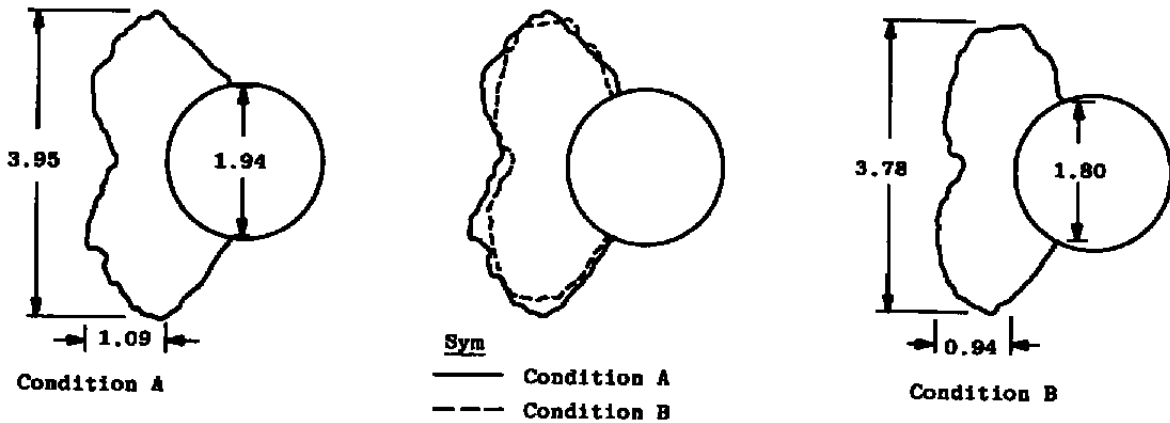
The above procedure was applied for each of the scaling methods to be evaluated. The tests were run on circular cylinders of 1- and 2-in.-diam and full-, 1/3-, and 1/6-scale airfoils at zero angle of attack. The airfoil section used for these tests was a supercritical airfoil with a reflexed trailing edge, as shown in Fig. 16. All cylinder and airfoil test articles were made of solid aluminum. The following sections describe the test facility and the procedures used to set the conditions during a test.

## 5.2 FACILITY DESCRIPTION

The experimental portion of this study was conducted in the ETF Research Test Cell (R-1D) at the AEDC. The icing research test cell (Fig. 17) consists of a flow-metering venturi, plenum chamber, water spray system, bellmouth, removable connecting ducts, and

a test chamber. Water droplets are sprayed into the primary air stream through a single, two-phase atomizing spray nozzle located in the plenum chamber, upstream of the bellmouth. The bellmouth terminates in a 12-in.-diam duct that directs the conditioned air to the test article in a 3-ft.-diam test section. A secondary air system supplies air to the test section that encapsulates the primary flow to prevent the recirculation of water droplets around the test article. The air is then exhausted to the atmosphere either directly or through the ETF exhaust plant.

2.0-in.-diam Cylinder



Dimension	Condition		Percent Error
	A	B	
Impingement Limit	1.94	1.80	7.3
Maximum Thickness	1.09	0.94	13.8
Maximum Width	3.95	3.78	4.3

Figure 15. Example of test cell and ice-accretion measurement repeatability.



Full-Scale Chord = 10.907 in.

Figure 16. Supercritical airfoil section used in the icing scaling studies.

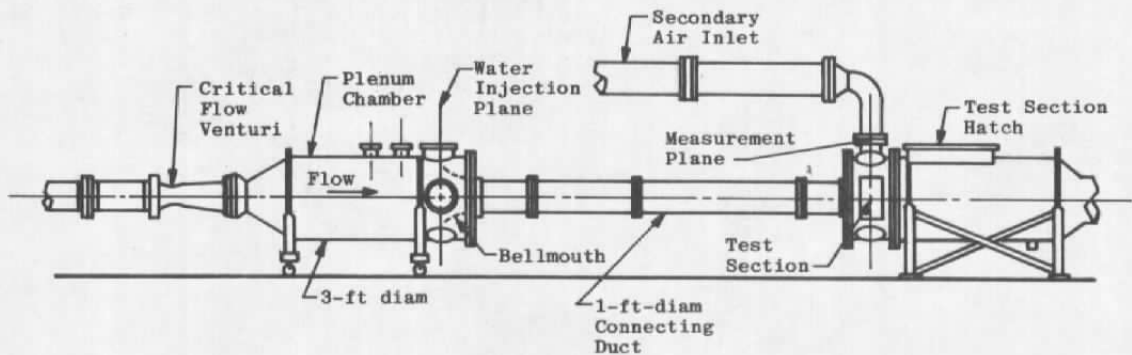


Figure 17. Icing research test cell.

This study requires that both the droplet size and LWC in the test section be accurately known and controlled. The methods used for specifying these parameters are described below.

### 5.2.1 Droplet Size Calibration

A two-phase atomizing spray nozzle is used to produce a cloud of water droplets in the test cell. A cloud with the desired mass median droplet size and spray water flow rate is obtained by setting the air and water pressures supplied to the spray nozzle. Each nozzle must, therefore, be calibrated prior to use in an icing test so that the droplet size corresponding to a given set of air and water pressures is known. The droplet size distribution in the cloud was measured using a fiber-optics particle-sizing system (FOS) developed at the AEDC. The FOS is an imaging device that uses a laser beam as a light source and an optical system to define a probe volume in the droplet flow field (Fig. 18). The probe volume is focused onto a linear array of sensor modules. As a droplet passes through the probe volume, its shadow occludes a number of the sensors. The number of sensors occluded is proportional to the droplet diameter. A thorough discussion of the operational theory of the FOS is given in Ref. 16.

The FOS has been compared with other particle diagnostic systems including a holographic imaging system (Ref. 17). Figure 19 shows a comparison of the mass median diameters of droplet size distributions obtained from the FOS and the spray nozzle calibration curve obtained from holographic data. Based on this and similar comparisons, the FOS is considered to provide accurate calibrations of droplet distributions produced by water spray nozzles.

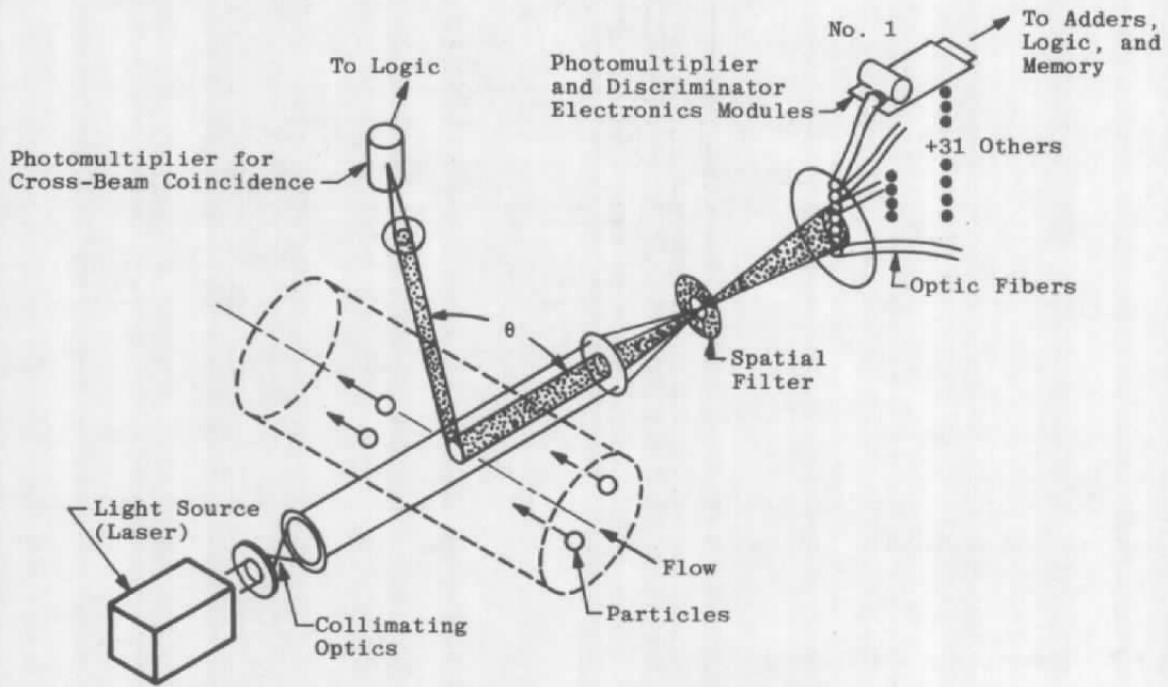


Figure 18. Fiber-optics particle-sizing system (Ref. 17).

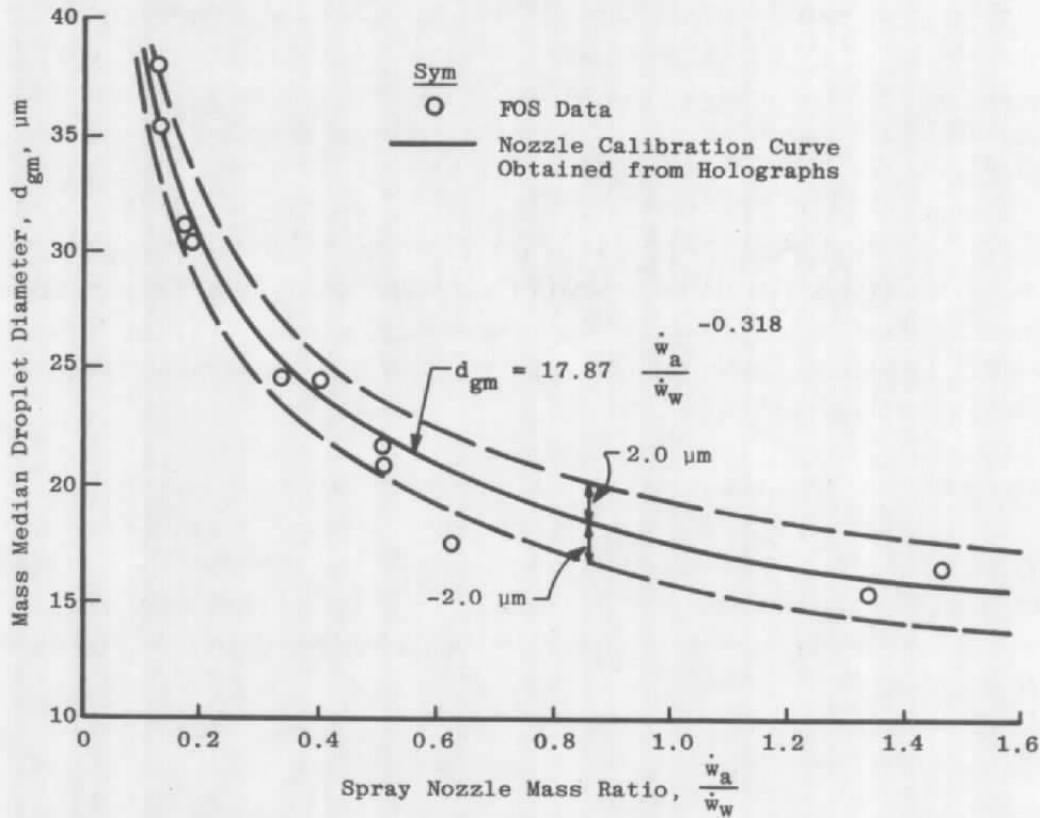


Figure 19. Comparison of FOS data with spray nozzle calibration (Ref. 17).

### 5.2.2 Determination of LWC

As with the droplet size measurement, the LWC is not measured on-line but is set by introducing the proper water flow into the air stream through the spray nozzle. Since the air received from the ETF air supply plant is essentially dry, considerable evaporation of the water could occur, thereby reducing the LWC. A computer code was developed at AEDC to calculate the amount of evaporation from droplets in a spray (Ref. 18) and was used to determine the additional amount of water that must be added to produce the required LWC in the test section. A comparison of methods used to determine the LWC in a test cell was done by Stallabrass (Ref. 19) and showed that the AEDC method provided the best comparison to measured values of LWC. Calibration of the icing research test cell has been achieved by comparing the LWC predicted by the AEDC method with the LWC calculated from holographic droplet-size measurements. These results, illustrated in Fig. 20, show that the input LWC agrees well with the measured values.

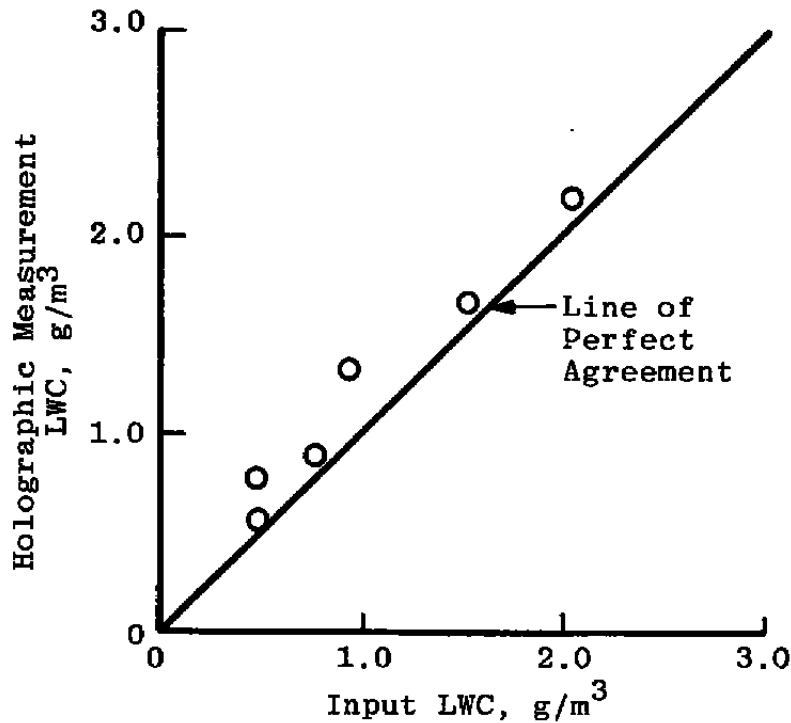


Figure 20. Comparison of input and measured LWC in the research test cell (Ref. 17).

### 5.3 TEST PROCEDURES

As discussed in Section 5.1, the aerodynamic and meteorological conditions to be run during a scaling test were determined using the computer code, SIMICE, so that the equations of the scaling method to be evaluated were satisfied. The spray nozzle pressures



required to produce the desired water flow rate (LWC) and mass median droplet diameter were determined from the appropriate nozzle calibration curves.

After a pretest calibration of all instrumentation was performed, the test cell pressure was reduced to the desired pressure altitude and primary and secondary inlet air was admitted to the test cell at the required pressure and temperature. Once the test cell flow conditions had stabilized to steady state, the desired water and air flows through the spray nozzle were set. Approximately 20 sec were required to stabilize the cloud on a desired condition.

After exposing the test article to the icing cloud for the desired length of time, the spray nozzle and primary air flow were stopped and the test cell brought to atmospheric pressure. The connecting duct section immediately in front of the test section (Fig. 17) was removed and the measurements of the ice accretions described in Section 5.1 were obtained. Approximately 5 min were required for this shutdown and measurement procedure. Since the test cell remained cold, no significant melting of the ice accretion was observed. This procedure was repeated for each test condition.

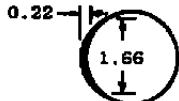
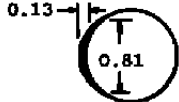
## 5.4 TEST RESULTS

The scaling methods previously discussed were evaluated beginning with the least restrictive, Method 1, and progressing to the most restrictive, Method 4. The ice-accretion profiles included here were redrawn to the same scale to allow direct comparisons. The dimensions shown on the profiles are those that were measured on the ice accretion.

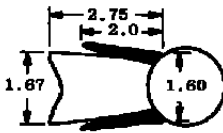
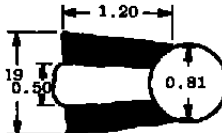
### 5.4.1 Method 1: $K_0$ and $A_c$ Constant

The static pressure and temperature were held constant for these cases, and the LWC and icing time were varied so that the value of  $A_c$  was maintained. The droplet diameter was calculated so that  $K_0$  was constant. Figure 21a compares rime ice accretions formed on a 2-in.-diam full-scale cylinder and a 1-in.-diam model at a static temperature = 0.0°F. The freezing fractions for these two cases are approximately 1.0 which is indicative of rime ice accretions. The ice shapes are similar indicating that this method appears to adequately scale results for rime ice accretions.

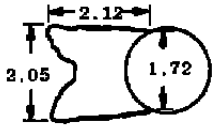
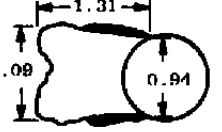
The accretions shown in Fig. 21b were also obtained at 0.0°F but at a greater velocity than the conditions in Fig. 21a. These accretions differ in shape, especially in the size of the rime feathers and glaze center portion. Note that the freezing fraction for the subscale model is greater than that of the full-scale model. This indicates that the subscale ice accretion should have a more rime-like character than the full-scale. This premise is evidenced by the

		LWC, g/m <sup>3</sup>	U <sub>∞</sub> , fps	T <sub>S</sub> , °F	P <sub>S</sub> , psia	$\bar{d}_m$ , μm	Time, min	K <sub>O</sub>	A <sub>c</sub>	n	b	$\phi$ , °F	$\theta$ , °F
Full-Scale 2.0-in.-diam		0.58	200	0	12.23	15.4	10	0.79	0.46	0.80	0.48	31.2	43.6
Model 1.0-in.-diam		0.57	200	0	12.23	10	5	0.77	0.46	1.0	0.33	31.3	35.3

a. Velocity = 200 fps, rime ice, test article size scaling

		LWC, g/m <sup>3</sup>	U <sub>∞</sub> , fps	T <sub>S</sub> , °F	P <sub>S</sub> , psia	$\bar{d}_m$ , μm	Time, min	K <sub>O</sub>	A <sub>c</sub>	n	b	$\phi$ , °F	$\theta$ , °F
Full-scale 2.0-in.-diam		0.36	366.7	0.68	12.23	22.3	30.6	2.08	1.59	0.70	0.51	28.78	39.01
Model 1.0-in.-diam		0.41	366.7	0.68	12.23	14.5	13.03	2.09	1.56	0.82	0.41	28.78	34.01

b. Velocity = 366.7 fps, mixed ice accretions, test article size scaling

		LWC, g/m <sup>3</sup>	U <sub>∞</sub> , fps	T <sub>S</sub> , °F	P <sub>S</sub> , psia	$\bar{d}_m$ , μm	Time, min	K <sub>O</sub>	A <sub>c</sub>	n	b	$\phi$ , °F	$\theta$ , °F
Full-Scale 2.0-in.-diam		1.2	200	5	14.0	31	15	2.33	1.42	0.41	1.18	26.2	35.6
Model 1.0-in.-diam		1.2	200	5	14.2	20	7.5	2.29	1.42	0.50	0.83	26.2	35.5

c. Velocity = 200 fps, mixed ice accretions, test article size scaling

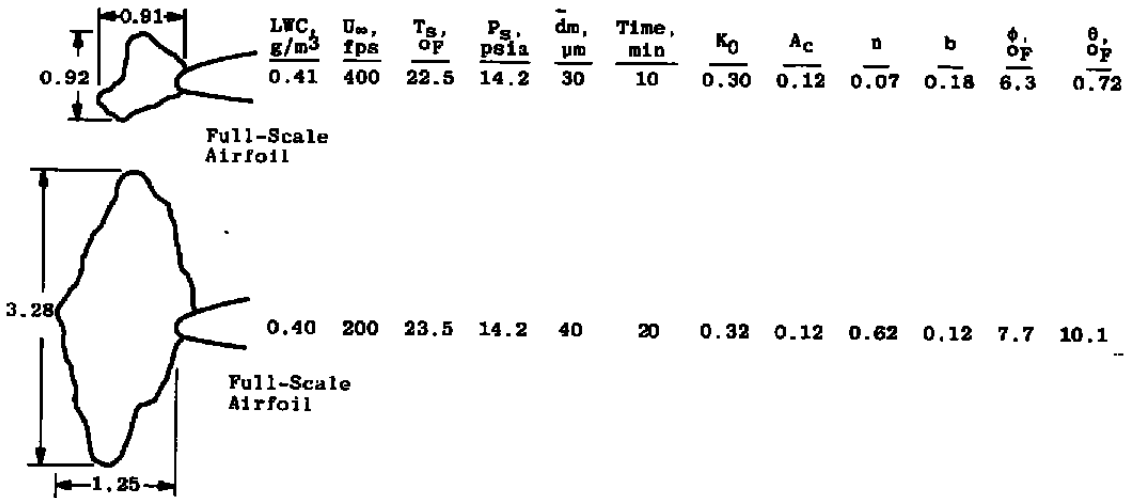
Figure 21. Comparison of rime, mixed, and glaze ice-accretion scaling using Method 1 to establish the experimental similitude conditions.

larger rime accretions on both sides of the glaze center. Similar conclusions can be drawn from the results shown in Fig. 21c. Note that the values of  $\phi$  and  $\theta$  are the same for the comparisons in Figs. 21b and 21c. This indicates that these two parameters are not sufficient for producing scaled ice shapes but still may be necessary, as will be examined in the evaluation of Method 4.

Figure 21d shows glaze accretions formed on two full-scale airfoils. In this set of conditions, the velocity was scaled from 400 to 200 fps and is an example of test parameter

scaling. The small amount of ice collected during the 400-fps condition indicates that it was near the icing onset, as evidenced by the low value of the freezing fraction.

From these results, it can be concluded that adequate scaling can be achieved using Method 1 only if the conditions are cold enough to produce a solid rime accretion. If any portion of the accretion has a glaze character, this method will not produce scaled ice shapes. These conditions also reemphasized the physical significance of the freezing fraction when considering the type of ice that will be formed.



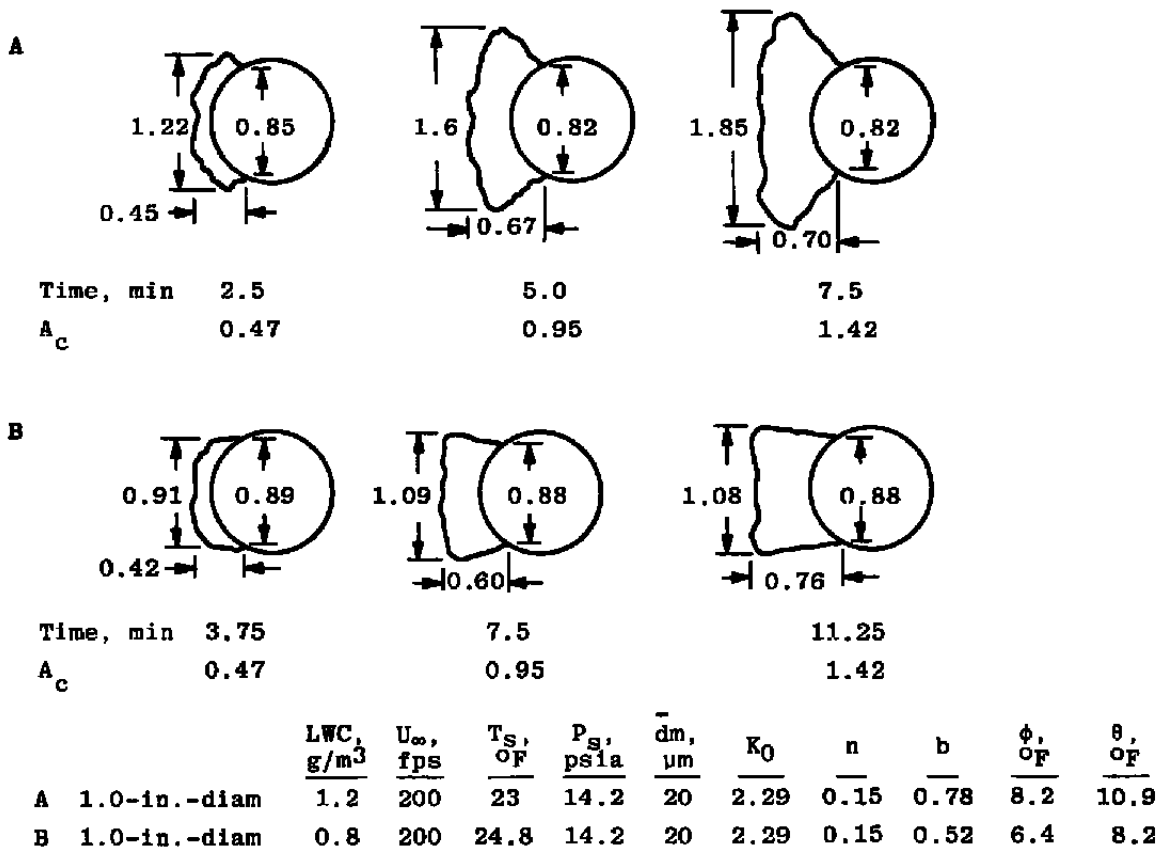
d. Airfoil glaze ice accretions, test parameter scaling  
Figure 21. Concluded.

5.4.2. Method 2: K<sub>0</sub> A<sub>c</sub>, and n Constant

Method 2 differs from Method 1 in that the free-stream static temperature of the model test condition is now calculated so that the freezing fraction is held constant. Figure 22a shows glaze ice accretions formed on two 1-in.-diam cylinders. The LWC was scaled from 1.2 to 0.8 g/m<sup>3</sup> while holding the freezing fraction constant. Both accretions are composed entirely of glaze ice, but the size and shape of the horns have not been accurately reproduced.

Figure 22b shows mixed ice accretions formed at the same condition as those in Fig. 22a except that the temperature was reduced. The profiles show some similarity at the short and intermediate times, but at the longest time, the differences between the accretions have become evident. The test conditions in Fig. 22c also show that the accretions appear similar for short times but become different as the accretion grows.

These results have shown that the Method 2 can ensure that the type of ice formed is the same, but the size and locations of the glaze horns are not adequately reproduced.



a. Cylinder glaze ice accretions test parameter scaling

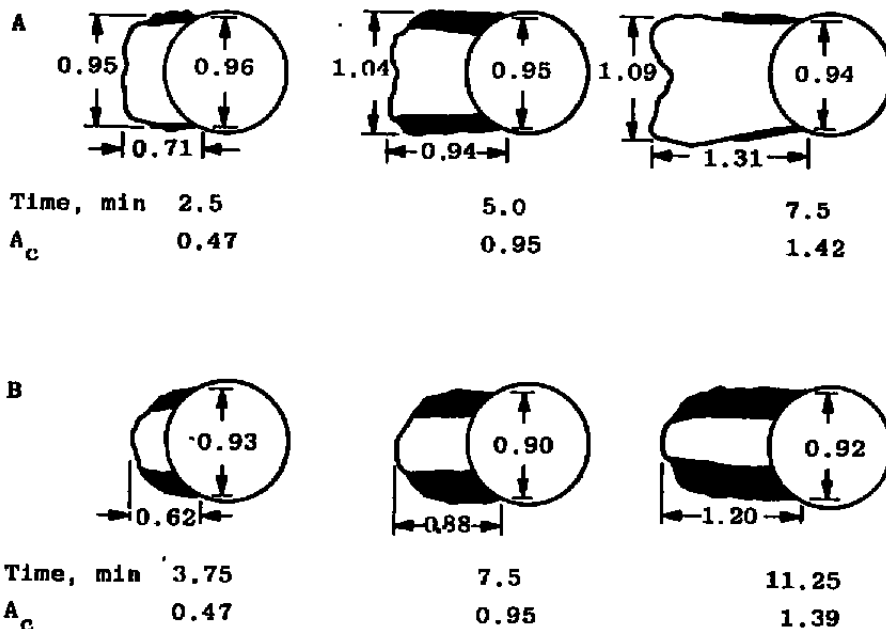
Figure 22. Comparison of glaze and mixed ice-accretion scaling using Method 2 to establish the experimental similitude conditions.

5.4.3 Method 3:  $K_0$ ,  $A_c$ ,  $n$ , and  $b$  Constant

In this method, the static temperature, droplet diameter, and icing time are determined as in Methods 1 and 2. The LWC at which the model is to be tested is calculated so that the relative heat factor is constant.

Figure 23a shows two glaze accretions formed on a full-scale airfoil. The static pressure was held constant as it would be in an atmospheric test facility, and the velocity was scaled from 200 to 350 fps. As in Method 2, the size of the glaze horns is not accurately reproduced. Figure 23b shows a condition for which the static pressure of the model

condition was specified to be 9.4 psia. Note that this still did not produce scaled ice accretions. Figure 23c, on the other hand, shows mixed ice accretions on two 1.0-in.-diam cylinders that were also formed at conditions with different pressures. The scaling of these two conditions, while not exact, is vastly improved over that in Figs. 23a and b.

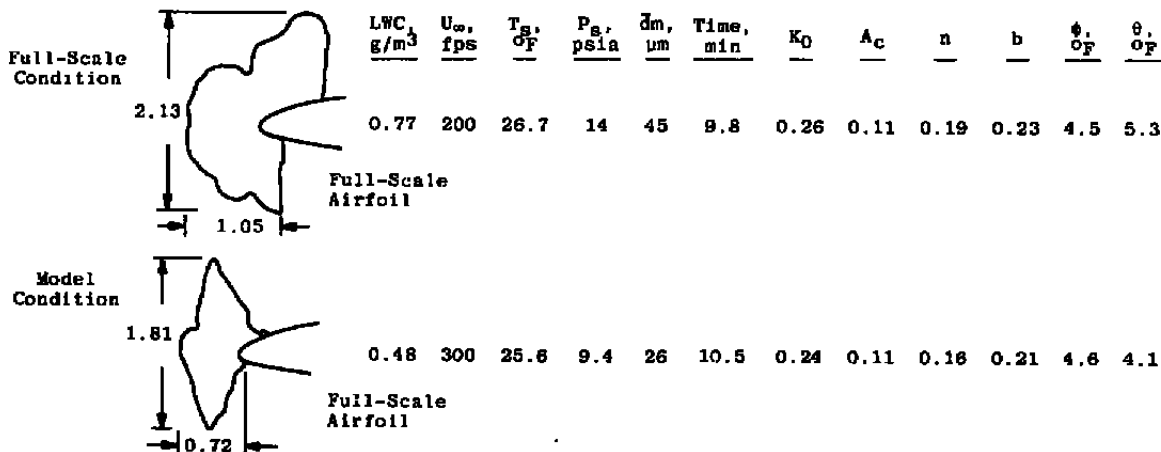


		$LWC, \frac{g}{m^3}$	$U_\infty, \frac{fps}{}$	$T_{S, OF}$	$P_S, \frac{psia}{}$	$\bar{d}_m, \frac{\mu m}{}$	$K_0$	$n$	$b$	$\phi, \frac{\phi}{OF}$	$\phi, \frac{\phi}{OF}$
A	1.0-in.-diam	1.2	200	5	14.2	20	2.29	0.50	0.83	26.2	35.5
B	1.0-in.-diam	0.8	200	11.5	14.2	20	2.29	0.50	0.54	19.7	27.2

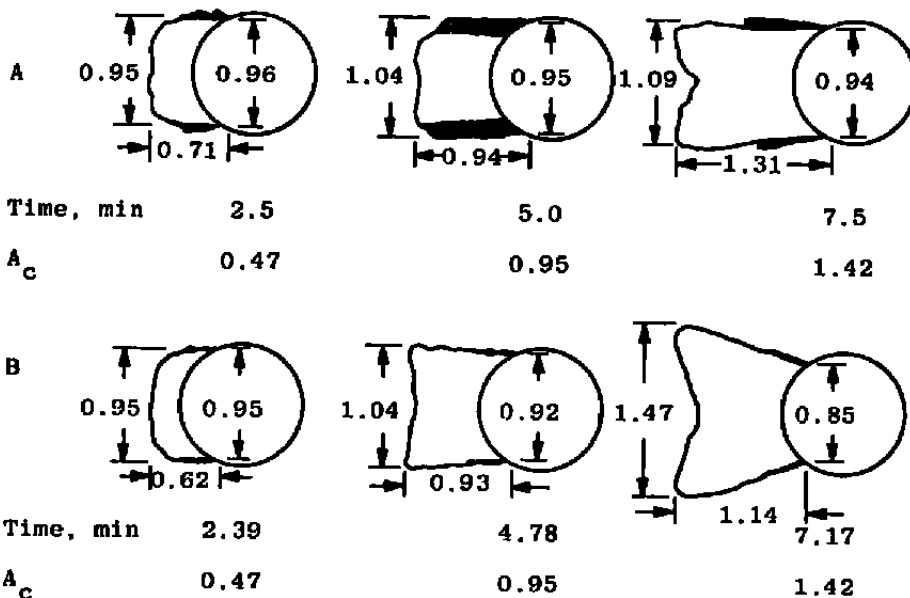
**b. Cylinder mixed ice accretions, test parameter scaling**  
**Figure 22. Continued.**

These results indicate that, with the proper selection of static pressure, this method may be able to produce scaled ice accretions. Since the additional knowledge about the relationship between the velocity and static pressure is not supplied by this method, accurate results cannot, in general, be obtained. It is interesting to note that the values of  $\phi$  and  $\theta$  are almost constant in Fig. 23c indicating that these may supply the additional information required to determine the correct static pressure.





**b. Airfoil glaze ice accretions, test parameter scaling**



		LWC, g/m <sup>3</sup>	U <sub>∞</sub> , fps	T <sub>S</sub> , °F	P <sub>S</sub> , psia	dm, μm	K <sub>O</sub>	n	b	φ <sub>OF</sub>	θ <sub>OF</sub>
A	1.0-in.-diam	1.2	200	5	14.2	20	2.29	0.50	0.83	26.2	35.5
B	1.0-in.-diam	0.8	313.9	5.2	10.1	15.4	2.26	0.47	0.82	24.9	34.4

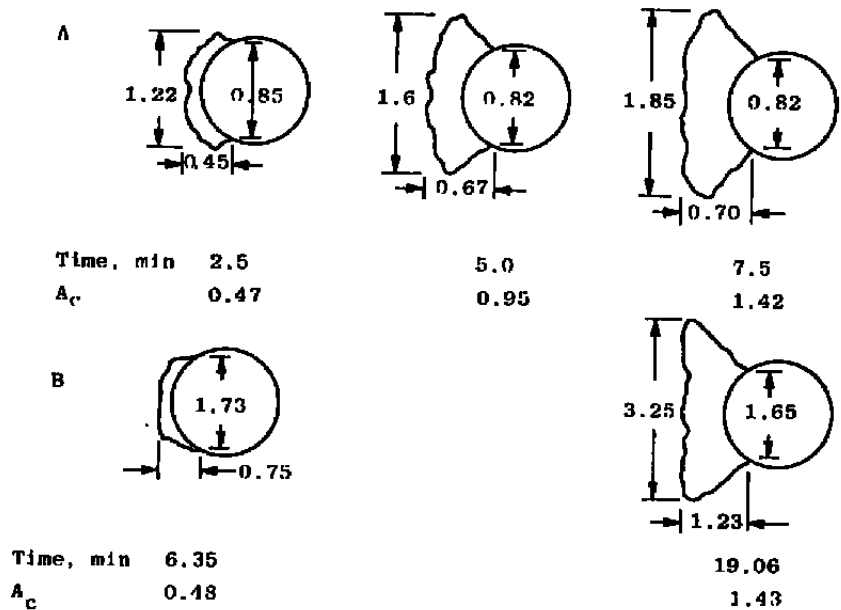
**c. Cylinder mixed ice accretions, test parameter scaling**

Figure 23. Concluded.

**5.4.4 Method 4:  $K_0$ ,  $A_c$ ,  $n$ ,  $\phi$ , and  $\theta$  Constant**

In this method, the static temperature and pressure are calculated so that  $\phi$  and  $\theta$  are held constant between the model and full-scale. Since the other icing parameters are calculated as in Method 2, only the model scale factor and free-stream velocity can be specified.

The results in Fig. 24a show that excellent similitude has been achieved between two glaze ice accretions. Note that the static pressures are different between the model and full-scale conditions and have been calculated so that  $\theta$  is held constant.



	LWC, $\frac{g}{m^3}$	$U_\infty$ , $\frac{fps}{}$	$T_s$ , $\frac{^{\circ}F}{}$	$p_s$ , $\frac{psia}{}$	$\bar{d}_m$ , $\frac{\mu m}{}$	$K_0$	$n$	$b$	$\frac{\phi}{\sigma_F}$	$\frac{\theta}{\sigma_F}$
A 1.0-in.-diam	1.2	200	23	14.2	20	2.29	0.15	0.78	8.2	10.9
B 2.0-in.-diam	0.76	250	22.6	12.7	27.5	2.28	0.14	0.83	8.1	10.1

**a. Cylinder glaze ice accretions, test article size scaling**

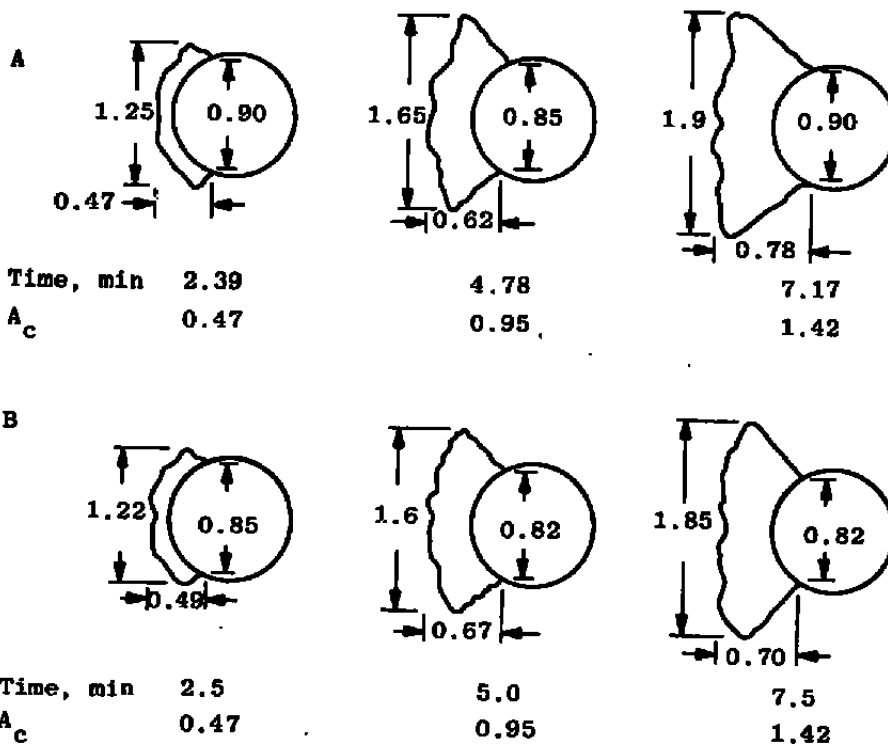
**Figure 24. Comparison of glaze and mixed ice-accretion scaling using Method 4 to establish the experimental similitude conditions.**

The comparison in Fig. 24b illustrates that scaled accretions can also be obtained for test parameter scaling. Condition A was obtained at a pressure altitude of 10,000 ft. The application of Method 4 allowed the condition to be scaled down to sea level, as shown in Condition B, so that the condition could be run in an atmospheric test facility.



This method also produced accurate scaling results for the mixed ice accretions on the full- and 1/3-scale airfoils shown in Fig. 24c. Note that even though the freezing fraction is calculated to be equal to 1.0, the ice in the center region has some glaze characteristics, namely the well-defined horns. This indicates that a calculated freezing fraction equal to 1.0 is not sufficient to ensure a smooth, aerodynamically shaped, rime ice accretion.

Figure 24d also shows well-scaled results for glaze ice accretions formed on the full- and 1/3-scale airfoils. The accretion on the 1/3-scale model is slightly smaller because, upon completion of the posttest analysis, the accumulation parameter was found to be less than that required for exact scaling. It is interesting to note that the accumulation parameters differed by 21 percent, and the maximum thickness of the ice accretions differed by 15

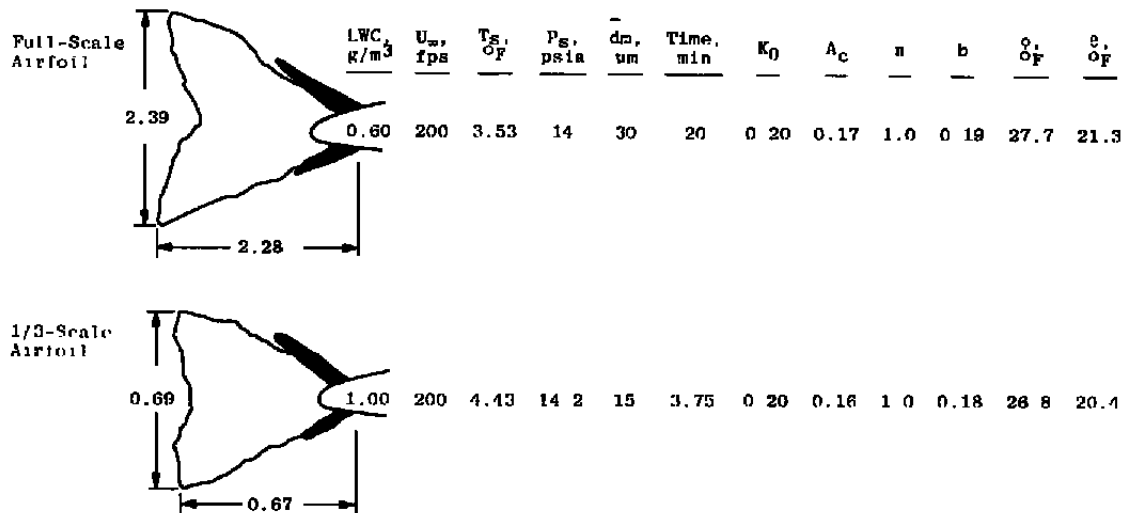


	LWC, g/m <sup>3</sup>	$U_\infty$ , fps	$T_{S, OF}$	$P_S$ , psia	$\bar{d}_m$ , $\mu\text{m}$	$K_0$	$n$	$b$	$\phi_{OF}$	$\theta_{OF}$
A 1.0-in.-diam	0.8	313.9	22	10.1	15.4	2.26	0.14	0.78	8.0	9.3
B 1.0-in.-diam	1.2	200	23	14.2	20	2.29	0.15	0.78	8.2	10.9

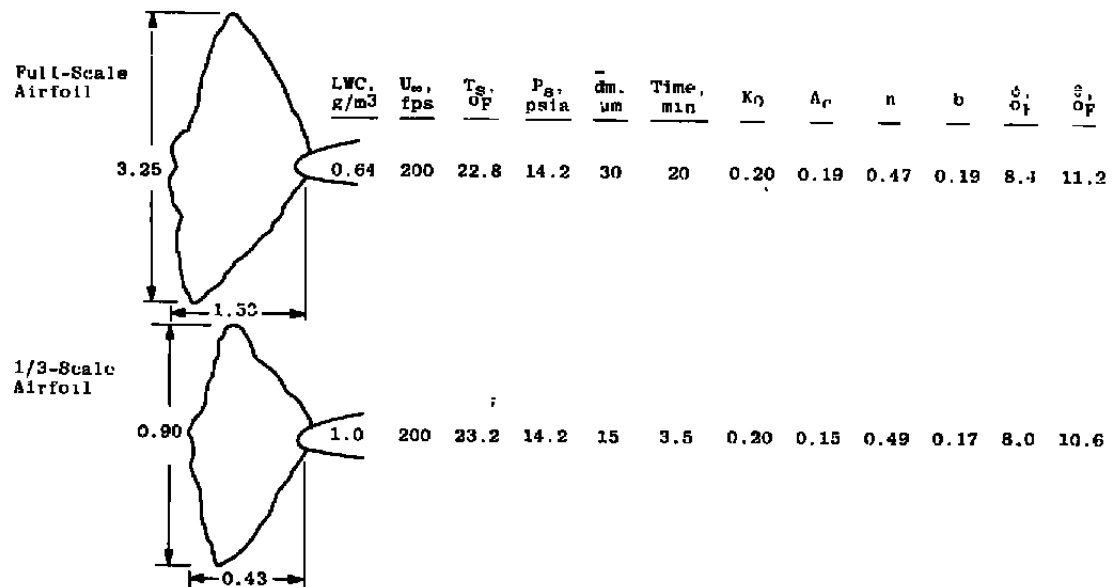
b. Cylinder glaze ice accretions, test parameter scaling

Figure 24. Continued.

percent. This illustrates the importance of the posttest calculation of the scaling parameters in the interpretation of scaling test data.



**c. Airfoil mixed ice accretions, test article size scaling**



**d. Airfoil glaze ice accretions, test article size scaling**

**Figure 24. Concluded.**

In all comparisons where this method was applied, the type and texture of the ice formed was similar. Comparison of the dimensions of the scaled shapes show that most dimensions

are geometrically scaled to within 10 percent. As was discussed in Section 5.1, since this scaling method produces results to the same order of accuracy as the repeatability of the measurement technique, it can be concluded that the method accurately scales the flow field, droplet impingement, and thermodynamic characteristics of the full-scale icing condition.

These results have identified a scaling procedure that accurately duplicates the ice-accretion profiles. In this scaling method,  $K_0$ ,  $A_c$ ,  $n$ ,  $\phi$ , and  $\theta$  are held constant. The set of verified scaling equations can, therefore, be expressed as follows:

$$1. (K_0)_{\text{model}} = (K_0)_{\text{full-scale}}$$

$$2. (A_c)_{\text{model}} = (A_c)_{\text{full-scale}}$$

$$3. (n)_{\text{model}} = (n)_{\text{full-scale}}$$

$$4. (\phi)_{\text{model}} = (\phi)_{\text{full-scale}}$$

$$5. (\theta)_{\text{model}} = (\theta)_{\text{full-scale}}$$

A final version of the icing scaling similitude code, SIMICE, was written to solve the above set of verified scaling equations (See AEDC-TR-85-30, Vol. II). The icing test parameters that must be determined from these equations are as follows:

1. velocity,
2. static pressure,
3. static temperature,
4. liquid-water content,
5. droplet diameter, and
6. icing time.

Note that there are six icing test parameters and only five equations, indicating that the problem is underspecified and that one of the test parameters can, therefore, be arbitrarily selected. In practice, this additional parameter is selected to overcome a test facility limitation. The solution of the above equations will be illustrated by two practical scaling examples to be discussed in the following section.

## 6.0 ICING SCALING APPLICATIONS

### 6.1 SAMPLE SCALING PROBLEMS

The experimental study has resulted in the verification of  $K_0$ ,  $A_c$ ,  $n$ ,  $\phi$ , and  $\theta$  as scaling parameters. The purpose of this section is to graphically illustrate the solution of the scaling equations for two icing test applications.

In these examples, it is desired to simulate the ice accretion that would be formed on a 36.0-in. chord NACA 0012 airfoil when exposed to the following icing condition:

geometry	= NACA 0012 airfoil
chord	= 36.0 in.
leading-edge diameter	= 1.14 in.
static temperature	= 25.0°F
static pressure	= 10.1 psia
velocity	= 200.0 fps
droplet diameter	= 20.0 $\mu\text{m}$
liquid-water content	= 0.5 g/m <sup>3</sup>
icing time	= 10.0 min

The icing similitude code, SIMICE, was used to evaluate the scaling parameters for the full-scale condition given above using the equations presented in the text. The results of these calculations are shown below.

$$\begin{aligned} K_0 &= 0.036 \\ A_c &= 0.013 \\ n &= 0.260 \\ \phi &= 6.190^\circ\text{F} \\ \theta &= 9.581^\circ\text{F} \end{aligned}$$

Two hypothetical test facilities, each of which has a limitation that does not allow the full-scale condition to be run, will be discussed in the following sample problems.

#### 6.1.1 Sample Problem 1: Test Article Size Scaling

The full-scale icing condition is to be simulated in a test facility where, because of blockage effects, the test article can have a maximum chord of 12.0 in. The scaling equations must be applied to determine the model icing conditions so that the ice-accretion shape will be simulated.

The scaling solution is begun by producing the plot of static temperature versus velocity shown in Fig. 25. This curve is constructed from Eq. (21) so that  $\phi$  has the same value as the full-scale icing condition, namely  $6.19^\circ\text{F}$ . Since one of the test parameters can be specified, let the velocity of the model test condition be 150.0 fps. At this velocity, Fig. 25 shows that the free-stream static temperature of the model condition should be  $25.4^\circ\text{F}$ .

The static pressure is now determined so that  $\theta$  is constant between the model and full-scale. Figure 26 shows the static pressures and velocities for which  $\theta$  is constant. Remember from Eq. (22) and Fig. 14 that  $\theta$  is also a function of the static temperature. Therefore, the static temperature is varying along the curve in Fig. 26 as a function of the velocity so that  $\phi$  is constant and equal to  $6.19^\circ\text{F}$  as shown in Fig. 25. For a velocity of 150.0 fps, the static pressure required for scaled ice shapes is found to be 12.2 psia. Note that for velocities below 100.0 fps, static pressures greater than sea-level static pressure are calculated.

The LWC can now be determined so that the freezing fraction is constant. Figure 27 shows values of LWC as a function of velocity for which the freezing fraction of the model condition is equal to that of the full-scale. Since both the static temperature and pressure are

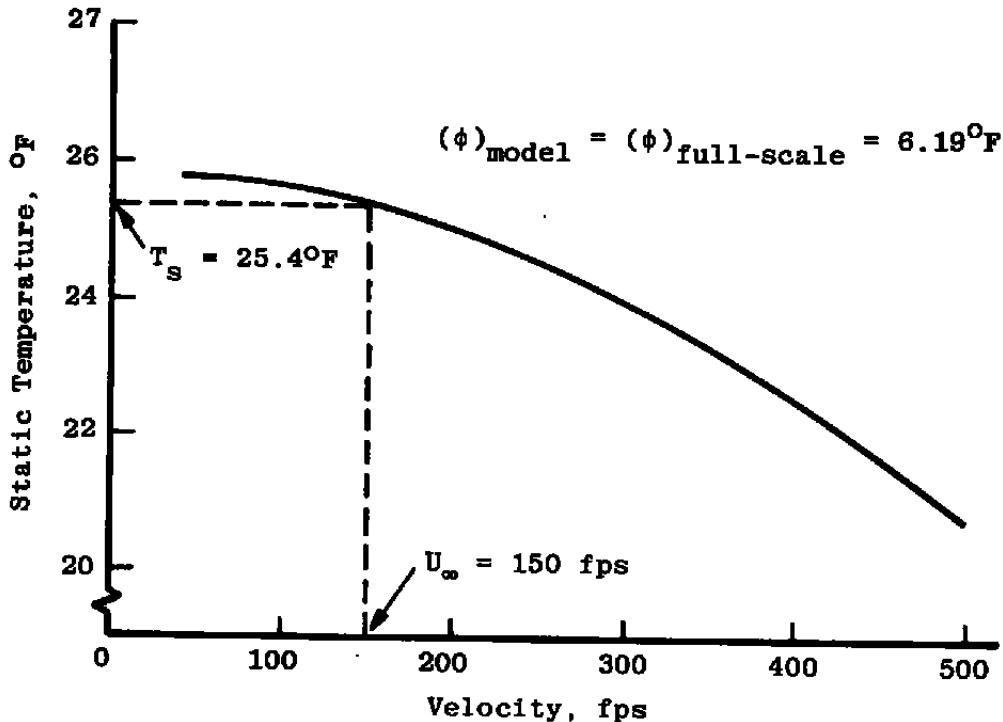
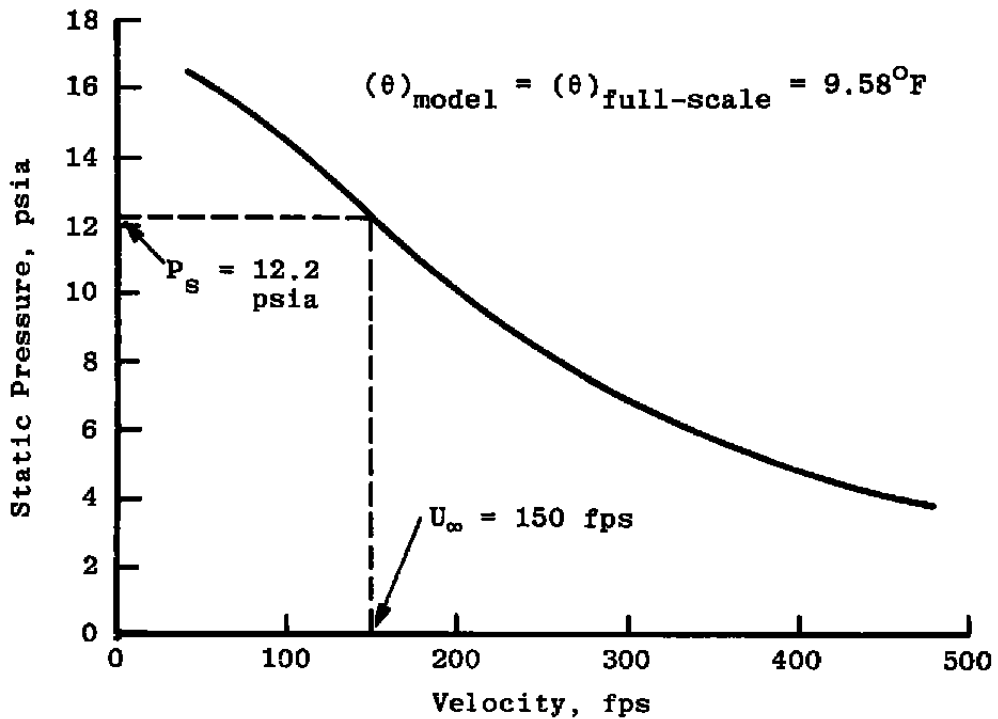


Figure 25. Sample Problem 1: Static temperature of the model condition as a function of model velocity for a constant value of droplet energy potential,  $\phi$ .



**Figure 26. Sample Problem 1: Static pressure of the model condition as a function of model velocity for a constant value of air energy potential,  $\theta$ .**

functions of velocity, they are also varying along this curve. Entering Fig. 27 with a velocity of 150.0 fps, the LWC required for the model test condition is found to be 1.10 g/m<sup>3</sup>.

Figures 28 and 29 are used in a similar manner to determine the mass median droplet diameter and the icing time so that the modified inertia parameter and accumulation parameter, respectively, are held constant.

By application of the scaling equations, the conditions at which the model should be tested to obtain a scaled ice shape have been found to be as follows.

velocity	= 150 fps
static pressure	= 12.2 psia
static temperature	= 25.4°F
LWC	= 1.10 g/m <sup>3</sup>
droplet diameter	= 12.1 μm
icing time	= 2.02 min

If, upon completion of this analysis, it was found that the LWC, say, was not obtainable at the required droplet diameter, the procedure would be repeated, starting with Fig. 25, with a new choice for the velocity and would be continued until a set of model conditions that could be run were obtained.

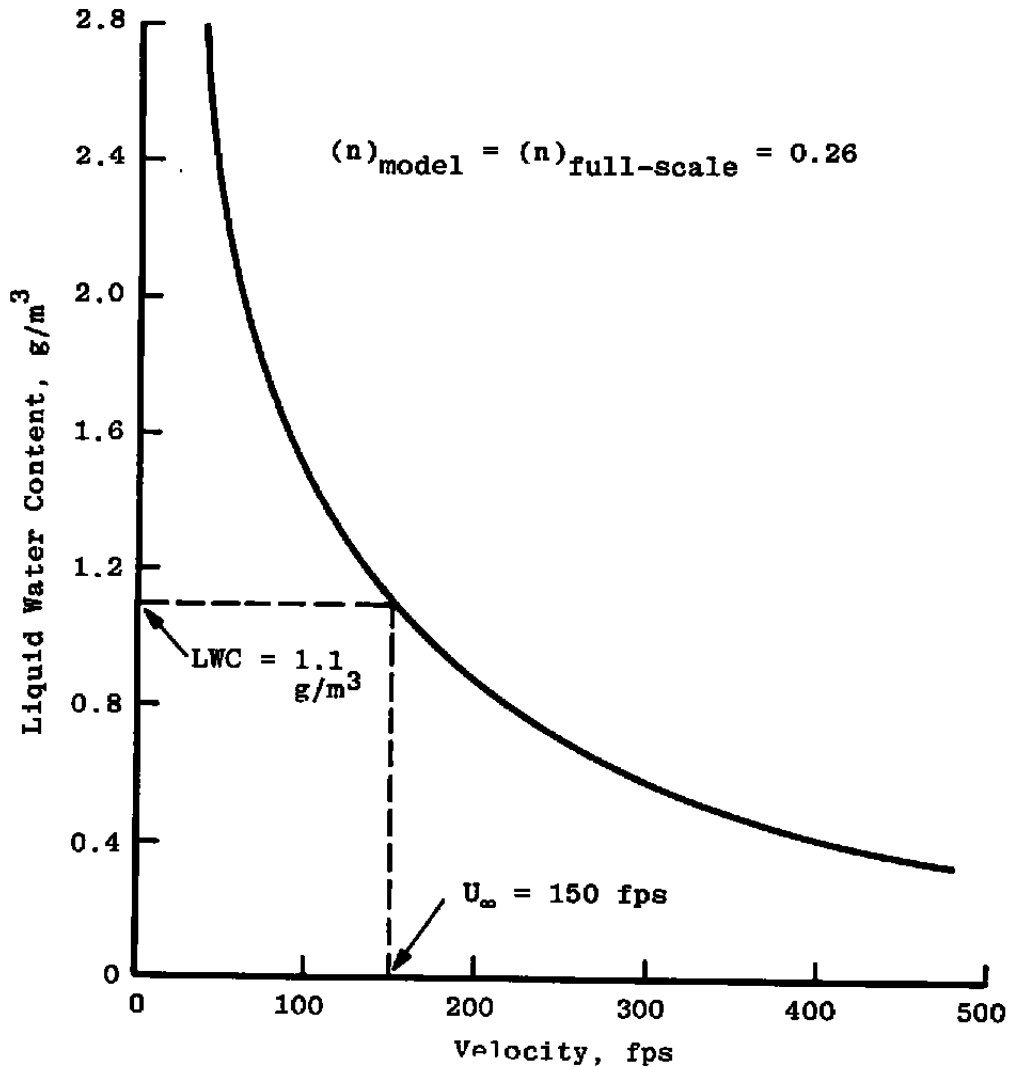


**Figure 27. Sample Problem 1: LWC of the model condition as a function of model velocity for a constant value of freezing fraction,  $n$ .**

### 6.1.2 Sample Problem 2: Test Parameter Scaling

In this example, the full-scale test condition is to be simulated in an atmospheric test facility in which the total pressure is constant and equal to the ambient pressure of 14.0 psia. The test facility is large enough so that the full-scale geometry can be tested.

Since  $\phi$  and  $\theta$  are independent of the model size, Figs. 25 and 26 are also applicable to this problem. Since there is now a restriction on the static pressure, the solution should be started in Fig. 26. In this example, it would be convenient to replot Fig. 26 in terms of the total pressure, as shown in Fig. 30. Entering Fig. 30 at 14 psia shows that a velocity of 114 fps is required for an accurate simulation. Figure 25 is then used as before to determine the required static temperature.

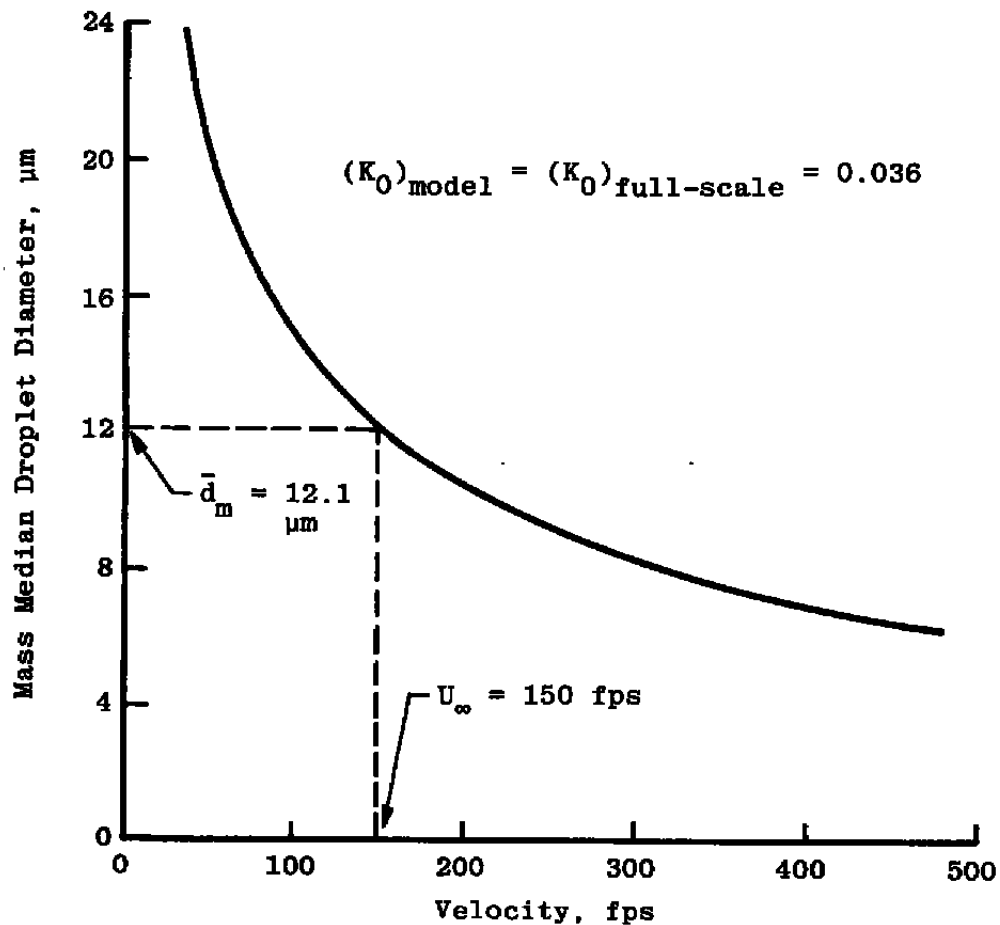


**Figure 28. Sample Problem 1: Mass median droplet diameter of the model condition as a function of model velocity for a constant value of modified inertia parameter,  $K_0$ .**

Since the velocity, pressure, and temperature are different from those in Sample Problem 1, it is necessary to calculate the LWC, droplet diameter, and icing time as functions of velocity to produce the plots shown in Figs. 31, 32, and 33, respectively. These are then used in the same manner as in Sample Problem 1 to determine the remaining test conditions. The solution to this sample scaling problem is as follows:



velocity = 114 fps  
 static pressure = 13.9 psia  
 static temperature = 25.6°F  
 LWC = 0.78 g/m<sup>3</sup>  
 droplet diameter = 26.7 μm  
 icing time = 11.3 min

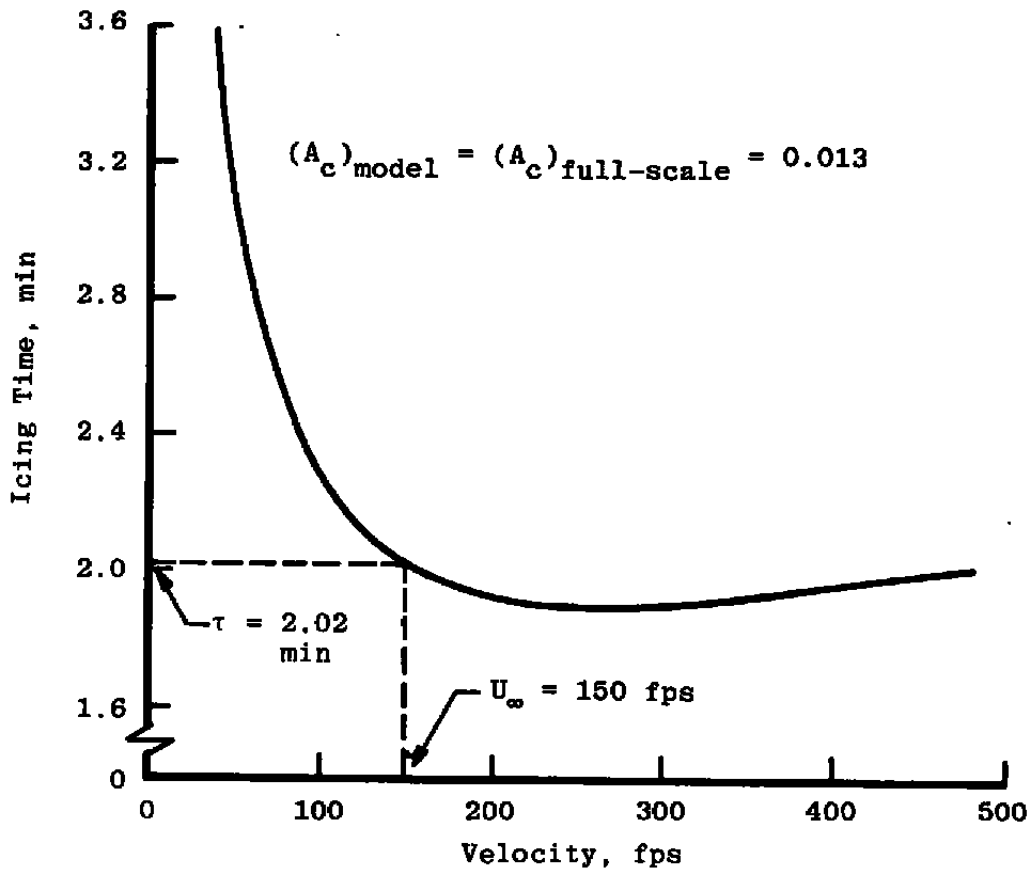


**Figure 29. Sample Problem 1: Icing time of the model condition as a function of model velocity for a constant value of accumulation parameter,  $A_c$ .**

Since the test facility has a strict pressure restriction, this is the unique solution at the required pressure that satisfies all the scaling equations for the full-scale article. If the facility cannot obtain one of the above conditions, for example, the droplet diameter at the required LWC, it would be necessary to consider reducing the size of the test article and attempting to find a solution at the reduced size. It must be realized that a condition that satisfies the scaling equations and is within the operational limits of the test facility may not exist.

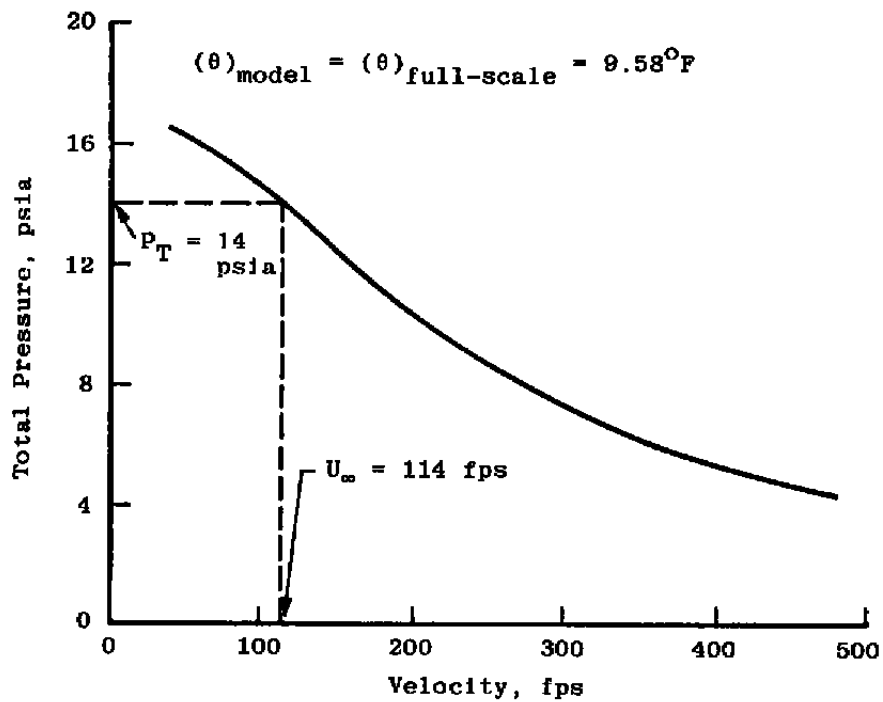


Figure 30. Sample Problem 2: Total pressure of the model as a function of model velocity for a constant value of air energy potential,  $\theta$ .

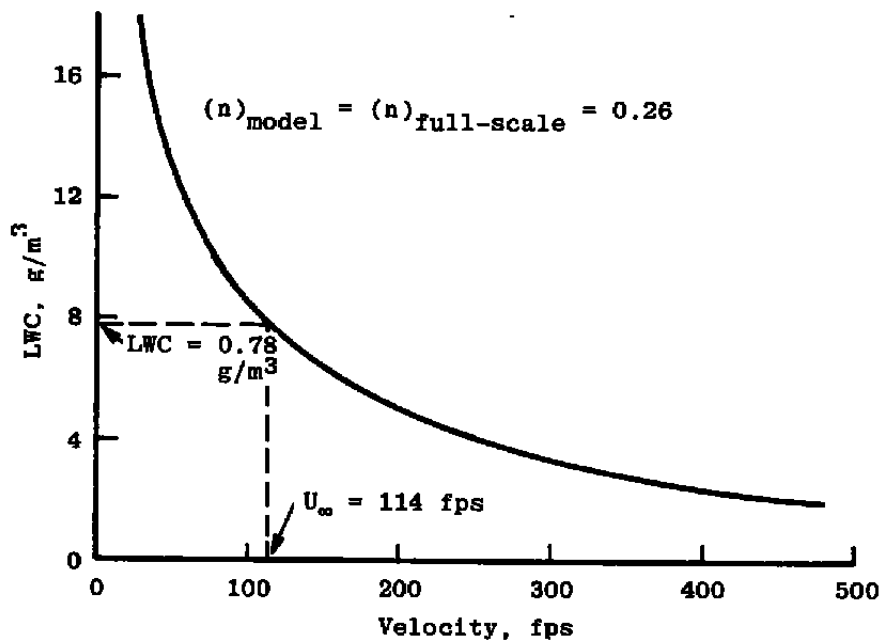


Figure 31. Sample Problem 2: LWC of the model condition as a function of model velocity for a constant value of freezing fraction,  $n$ .

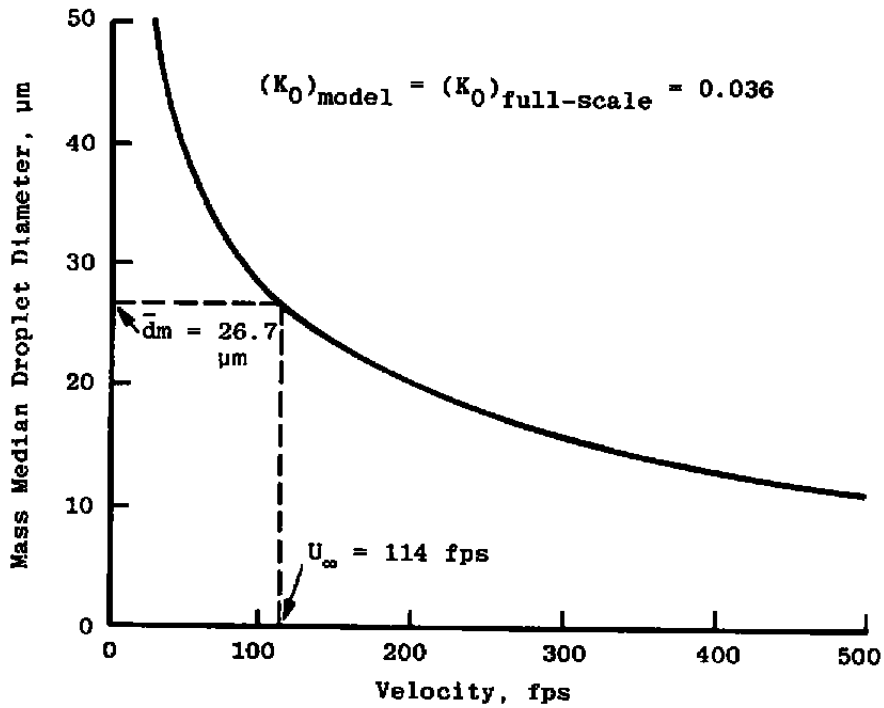


Figure 32. Sample Problem 2: Mass median droplet diameter of the model condition as a function of model velocity for a constant value of modified inertia parameter,  $K_0$ .

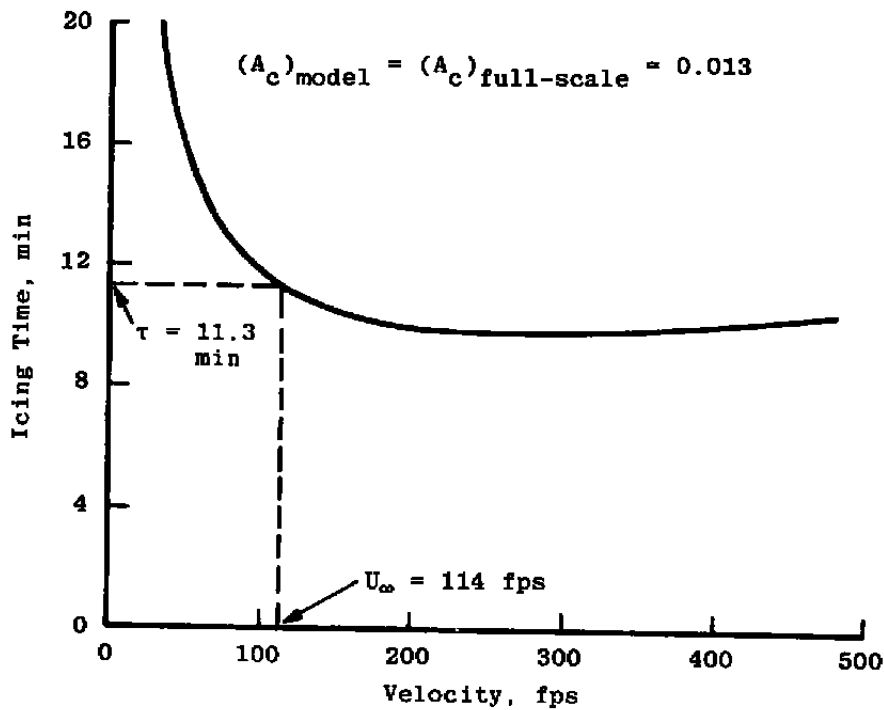


Figure 33. Sample Problem 2: Icing time of the model condition as a function of model velocity for a constant value of accumulation parameter,  $A_c$ .

The previous examples have illustrated the solution to two practical scaling problems. The icing similitude computer code, SIMICE, was used to produce the figures shown in this section.

## 7.0 LIMITATIONS

### 7.1 VELOCITY SCALING LIMITATIONS

#### 7.1.1 Critical Mach Number

As discussed in Section 3.1, the critical Mach number of the test geometry serves as the upper limit for velocity scaling because the character of the flow field changes. This limit also exists in the droplet trajectory calculations because the effects of compressibility are no longer negligible (Ref. 20). Therefore, scale accretions cannot be expected if the velocity is scaled above  $M_c$ . If velocity scaling is desired with both velocities greater than or equal to  $M_c$ , the droplet trajectories for each velocity should be calculated to determine if there are significant differences caused by compressibility. If necessary, relationships that express the stagnation-line collection efficiency as a function of modified inertia parameter must be calculated.

#### 7.1.2 Ice Shedding

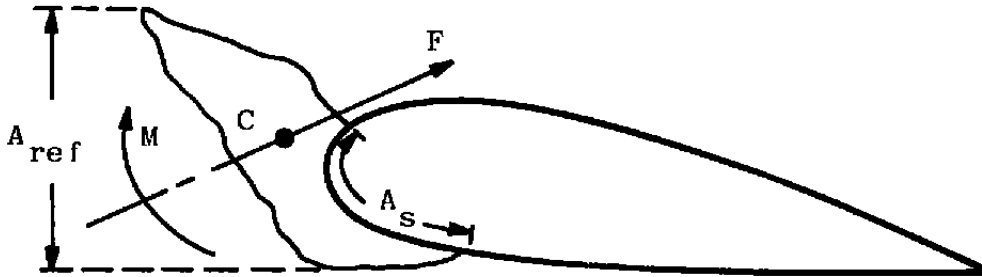
The experimental results have shown that ice accretions with similar appearance can be obtained through the application of velocity scaling. The shedding of ice accretions imposes limits on velocity scaling that are more restrictive than the critical Mach number limit described above.

Ice will shed from an object when the shear stress between the ice and the surface or within the ice structure itself reaches some critical value which is dependent on the conditions at which the ice was formed. Since the model and full-scale ice accretions are formed under similar thermodynamic processes, the critical values of the shear stress will be nearly identical. The stress within the ice is a result of the drag and moment forces on the ice accretion itself, as shown in Fig. 34. The magnitude of these forces are dependent on the size of the accretion, static pressure, and free-stream velocity.

Since the forces are proportional to the dynamic pressure,  $q = 1/2 \gamma P_s M^2 = 1/2 \rho_a U_\infty^2$ , an equivalent force,  $F$ , can be defined such that the shear stress at the surface of the airfoil can be expressed as

$$\sigma = \frac{F}{A_s} = c_{Di} \frac{1}{2} \frac{\rho_a U_\infty^2 A_{ref}}{A_s} \quad (29)$$

where  $c_{D_i}$  is a total drag coefficient that can be attributed to the ice accretion and is a function of the shape of the ice accretion. The areas  $A_{ref}$  and  $A_s$  are defined in Fig. 34. Since the full- and subscale ice accretions have similar profiles and surface characteristics, the values of  $c_{D_i}$  will be similar assuming the effects of the difference in Reynolds number to be small.



- C = Centroid of the Ice Accretion Cross-Sectional Area
- $A_{ref}$  = Reference Dimension for the drag coefficient,  $c_{D_i}$
- $A_s$  = Area of Attachment
- F = Aerodynamic Force Acting Through the Centroid
- M = Moment of the Ice Accretion About the Centroid

**Figure 34. Definition of icing shedding analysis terms.**

Suppose that a full-scale accretion has been formed at a velocity  $U_1$  and obtained a value of  $c_{D_i}$  such that the critical shear stress has just been reached, i.e. shedding is imminent. The shear stress at that time is

$$\sigma_c = c_{D_i} \frac{1}{2} \frac{\rho_a U_1^2 A_{ref}}{A_s} \tag{30}$$

A subscale accretion will have the same value of  $c_{D_i}$  and same ratio of  $A_{ref}/A_s$ , but since it has been formed at a lower velocity, the shear stress will not be near the critical value. While many simplifying assumptions have been made, this analysis does show that (1) testing at lower velocities can allow ice shapes to grow larger than they would on a full-scale geometry, and (2) it may be possible to scale the shedding characteristics by holding the dynamic pressure constant.

At the time this experimental study was conducted, the icing research test cell was not capable of adequately evaluating this proposed scaling requirement because of air mass flow rate limitations. Limited results did reveal that above approximately  $M = 0.4$  at a static

pressure of 14.2 psia ( $q = 1.6$  psia) shedding played a significant role in the ice-accretion process and affected the final shape of the ice accretion. Therefore, without verification of the dynamic pressure scaling requirement, scaling from a full-scale dynamic pressure,  $q_f$ , greater than 1.6 psia to a model dynamic pressure,  $q_m$ , less than 1.6 psia or vice versa is not recommended. Accurate velocity scaling with both  $q_f$  and  $q_m$  greater than or less than 1.6 psia without setting  $q_m = q_f$  can be accomplished only if the time to shed for either ice accretion has not been exceeded.

Analytically predicting the time to shed is dependent on the ability to evaluate (1) the change in drag and moment coefficient as functions of time, and (2) the critical shear stresses between the ice and the surface and within the ice itself. These parameters are also functions of the aerodynamic and meteorological conditions at which the accretion was formed and are beyond the present capabilities of icing analysis. Only test results and empirical correlations can currently provide direction in defining these limits.

## 7.2 GENERAL LIMITATIONS

The ranges over which the atmospheric and meteorological parameters were tested are shown in Table 3. These limits are the result of facility limitations and not of the scaling

**Table 3. Ranges of Test Parameters Investigated at the AEDC**

Parameter	Low	High
Velocity, fps	100	400
Static Pressure, psia	4.4	14.2
Static Temperature, °F	-5	32
LWC, g/m <sup>3</sup>	0.26	1.54
Droplet Diameter, $\mu$ m	10	45
Icing Time, min	1.5	31.0
Model Scale Factor	0.17	6.0

equations themselves. The test results did not indicate that any of these were physical limits of the scaling equations. With the possible exception of velocity, these ranges adequately cover a large portion of the icing test envelopes required by aircraft manufacturers.

## 8.0 SUMMARY OF RESULTS

The objectives of this study were to evaluate the equations governing the ice-accretion process to identify proposed scaling parameters and to conduct tests to determine which, if any, of the proposed methods produced scale ice accretions. A set of scaling equations were verified, and limitations of the scaling techniques were identified. A computer code was developed to solve the scaling equations for use in various icing applications. The results of this study can be summarized as follows:

1. A set of equations that can be used to calculate test conditions so that scaled ice shapes are produced on geometrically similar bodies was developed and experimentally verified. The test conditions are such that  $K_0$ ,  $A_c$ ,  $n$ ,  $\phi$ , and  $\theta$ , are held constant.
2. The posttest evaluation of the scaling parameters based on the actual test conditions was necessary for the accurate evaluation of test results.
3. An icing similitude computer code, SIMICE, was developed to calculate similitude conditions using the verified scaling equations.
4. The equations are applicable over the range of meteorological conditions found in natural icing, with the possible exception of velocity.
5. Velocity is the primary limitation of the scaling equations. To maintain scaled flow fields and droplet impingement characteristics, both the model and full-scale velocities must yield a Reynolds number greater than or equal to  $2.0 \times 10^5$  and less than the velocity giving the critical Mach number of the body geometry.
6. At values of dynamic pressure of approximately 1.6 psia, the shedding characteristics of the ice accretion were observed to effect the final ice shape. Therefore, ice accretions did not scale well when  $q_f > 1.6$  psia and  $q_m < 1.6$  or vice versa.
7. A method for scaling shedding characteristics by maintaining the dynamic pressure was developed, but facility limitations did not permit adequate verification. Additional testing is required to verify this ice-shedding scaling technique.

## REFERENCES

1. Pope, A. *Wind Tunnel Testing*. John Wiley and Sons, Inc., New York, 1947.
2. Bragg, M. B., Gregorek, G. M., and Shaw, R. J. "An Analytical Approach to Airfoil Icing." AIAA Paper No. 81-0403, Presented at the 19th Aerospace Sciences Meeting, January 12-15, 1981.
3. Langmuir, E. and Blodgett, K. B. "A Mathematical Investigation of Water Droplet Trajectories." General Electric Co., ATI 25-223, February 1946.
4. Bowden, D. T., Gensemer, A. E., and Skeen, C. A. "Engineering Summary of Airframe Icing Technical Data." Federal Aviation Agency FAA-ADS-4, March 1964.
5. Frost, W., Chang, H. P., and Kimble, K. R. "Particle Trajectory Computer Program for Icing Analysis." Final report for NASA/Lewis Research Center Under Contract NASA-22442 by FWG Associates, Inc., April 1982.
6. Chang, H. P., Frost, W., and Shaw, R. J. "Influence of Multidroplet Size Distribution on Icing Collection Efficiency." Presented at the AIAA 21st Aerospace Sciences Meeting, AIAA Paper No. 83-0110, January 10-13, 1983.
7. Olsen, W. "Close-up Movies of the Icing Process on the Leading Edge of an Airfoil." NASA/Lewis Research Center Movie C-313, 1985.
8. Tribus, M. V. et. al. "Analysis of Heat Transfer Over a Small Cylinder in Icing Conditions on Mount Washington." American Society of Mechanical Engineers—Transactions, Vol. 70, 1949, pp. 871-876.
9. Messinger, B. L. "Equilibrium Temperature of an Unheated Icing Surface as a Function of Airspeed." *Journal of the Aeronautical Sciences*, Vol. 20, No. 1, January 1953, pp. 29-42.
10. Fergus, J. L., Jr. "A Steady-State Thermal Model for Analysis of Incipient Icing on an Airfoil Leading Edge." AEDC-TR-83-2 (AD-A131207), July 1983.
11. Sibley, P. J. and Smith, R. E., Jr. "Model Testing in an Icing Wind Tunnel." Lockheed Aircraft Corporation, Report No. LR10981, 1955.



12. Jackson, E. T. "Development Study: The Use of Scale Models in an Icing Tunnel to Determine the Ice Catch on a Prototype Aircraft with Particular Reference to Concorde." British Aircraft Corporation (Operating) Ltd., Filton Division, SST/B75T/RMMcK/242, July 1967.
13. Armand, C. et. al. "Techniques and Facilities Used at the Onera Modane Centre for Icing Tests." North Atlantic Treaty Organization Advisory Group for Aerospace Research and Development, AGARD-AF-127, November 1978.
14. Hauger, H. H. and Englar, K. G. "Analysis of Model Testing in an Icing Wind Tunnel." Douglas Aircraft Company, Inc. Report No. SM14933, 1954.
15. Dodson, E. O. "Scale Model Analogy for Icing Tunnel Testing." Boeing Airplane Company, Transport Division, Document No. D66-7976, March 1962.
16. Bentley, H. T. "Fiber Optics Particle-Sizing System." AEDC-TR-73-111 (AD-766647), September 1973.
17. Hunt, J. D. "A Comparison of Particle Diagnostic Systems." AEDC-TR-80-33 (AD-A104027), August 1981.
18. Willbanks, C. E. and Schulz, R. J. "Analytical Study of Icing Simulation for Turbine Engines in Altitude Test Cells." AEDC-TR-73-1444 (AD-770069), November 1973.
19. Stallabrass, J. R. "Procedure for Allowing for the Evaporation from Water Droplets in an Engine Icing Test Cell." National Research Council of Canada (NRC) Report LTR-LT-129, January 1982.
20. Brun, R. J., Serafini, J. S., and Gallagher, H. M. "Impingement of Cloud Droplets on Aerodynamic Bodies as Affected by Compressibility of Air Flow Around the Body." NACA TN 2903, March 1953.

## APPENDIX A

### DERIVATION OF THE MODIFIED INERTIA PARAMETER

The droplet trajectory equation was given in the text as

$$m_d \left( \frac{d^2 \bar{x}}{dt^2} \right) = \bar{D} \quad (\text{A-1})$$

Further simplification of this equation is made by assuming that the droplets are spherical. Approximating droplets as rigid spheres is valid for drop radii less than 500  $\mu\text{m}$  (Ref. A-1).

The drag force for a sphere in Stokes' flow ( $R < 1.0$ ) is given by the equation

$$\bar{D}_{\text{Stokes}} = 6\pi \mu_a r_d (\bar{U}_a - \bar{U}_d) \quad (\text{A-2})$$

Since most droplet flow occurs outside this range, a correction must be made to account for deviations from Stokes' Law. This correction has the form

$$\bar{D} = 6\pi \mu_a r_d (\bar{U}_a - \bar{U}_d) \frac{C_D R}{24} \quad (\text{A-3})$$

When Stokes' Law is applicable,  $C_D(R)/24 = 1.0$ , and the drag force is equal to  $\bar{D}_{\text{Stokes}}$ . Under other conditions,  $C_D(R)/24 < 1.0$ , and accounts for deviations from Stokes' Law.

The effect of gravity on the trajectories of droplets less than 50.0- $\mu\text{m}$  is usually negligible and, therefore, is omitted in most icing studies (Ref. A-2). With these simplifications, the droplet trajectory equation becomes

$$K \left( \frac{d\bar{U}_d'}{dt'} \right) = \frac{C_D R}{24} (\bar{U}_a - \bar{U}_d) \quad (\text{A-4})$$

Note that two nondimensional parameters have appeared in Eq. (A-4). The first is the droplet Reynolds number,  $R$ , expressed as

$$R = \frac{\rho_a d |\bar{U}_a - \bar{U}_d|}{\mu_a} \quad (\text{A-5})$$

The second is the inertia parameter,  $K$ , which can be expressed as

$$K = \frac{2}{9} \frac{\rho_w r_d^2 U_\infty}{\mu_a c} \quad (\text{A-6})$$

where  $c$  is the characteristic length of the body geometry, i.e. airfoil chord or cylinder radius.

Since all the terms in the equation are now nondimensional, solutions for equal values of  $K/(C_D R/24)$  will be identical, assuming that the requirement for identical flow fields has been satisfied. This term is not constant throughout the trajectory calculation since  $R$  is based on the velocity difference between the gas and the droplet. Therefore, a representative value of  $K/(C_D R/24)$  that is unique for given trajectory will serve as a droplet scaling parameter.

Langmuir (Ref. A-3) used an average value of  $C_D(R)/24$  to represent each trajectory in his analysis. This average was defined as the range parameter,  $\lambda/\lambda_s$ , and can be expressed by the following equation:

$$\lambda/\lambda_s = \frac{1}{R_u} \int_0^{R_u} \frac{24}{C_D R} dR \tag{A-7}$$

where  $R_u$  is the droplet Reynolds number based on the free-stream velocity,  $U_\infty$ . If values of  $C_D$  as a function of  $R_u$  are known, this equation can be integrated to produce values of  $\lambda/\lambda_s$  as a function of  $R_u$  as shown by the plot in Fig. A-1. The modified inertia parameter,  $K_0$  is then defined as

$$K_0 = (\lambda/\lambda_s) K \tag{A-8}$$

An alternate approach proposed by Bragg (Ref. A-2) used the value of  $C_D R/24$  corresponding to  $R_u$  instead of the average used by Langmuir. In this case, the scaling parameter becomes

$$\bar{K} = \frac{K}{(C_D R_u/24)} \tag{A-9}$$

By substituting an expression for  $C_D$  of the form  $C_D = R_u^\gamma$ , Eq. (A-9) becomes

$$\bar{K} = \frac{c \rho_a^{1+\gamma} d^{\gamma-1} U_\infty^\gamma}{e_w \mu_a^\gamma} \tag{A-10}$$

and is solved by substituting the value of  $\gamma$  that best fits the  $C_D$  versus  $R_u$  curve in the desired Reynolds number range.

Although both of these methods have been shown to adequately scale droplet trajectories, the method of Langmuir was used in the current study because all of the past droplet impingement data have been plotted as function  $K_0$ .

#### REFERENCES

- A-1. Hobbs, P. V. *Ice Physics*. Oxford University Press, Ely House, London, 1974.
- A-2. Bragg, M. B., Gregorek, G. M., and Shaw, R. J. "An Analytical Approach to Airfoil Icing." AIAA Paper No.81-0403, Presented at the 19th Aerospace Sciences Meeting, January 12-15, 1981.
- A-3 Langmuir, E. and Blodgett, K. B. "A Mathematical Investigation of Water Droplet Trajectories." General Electric Co., ATI 25 223, February 1946.

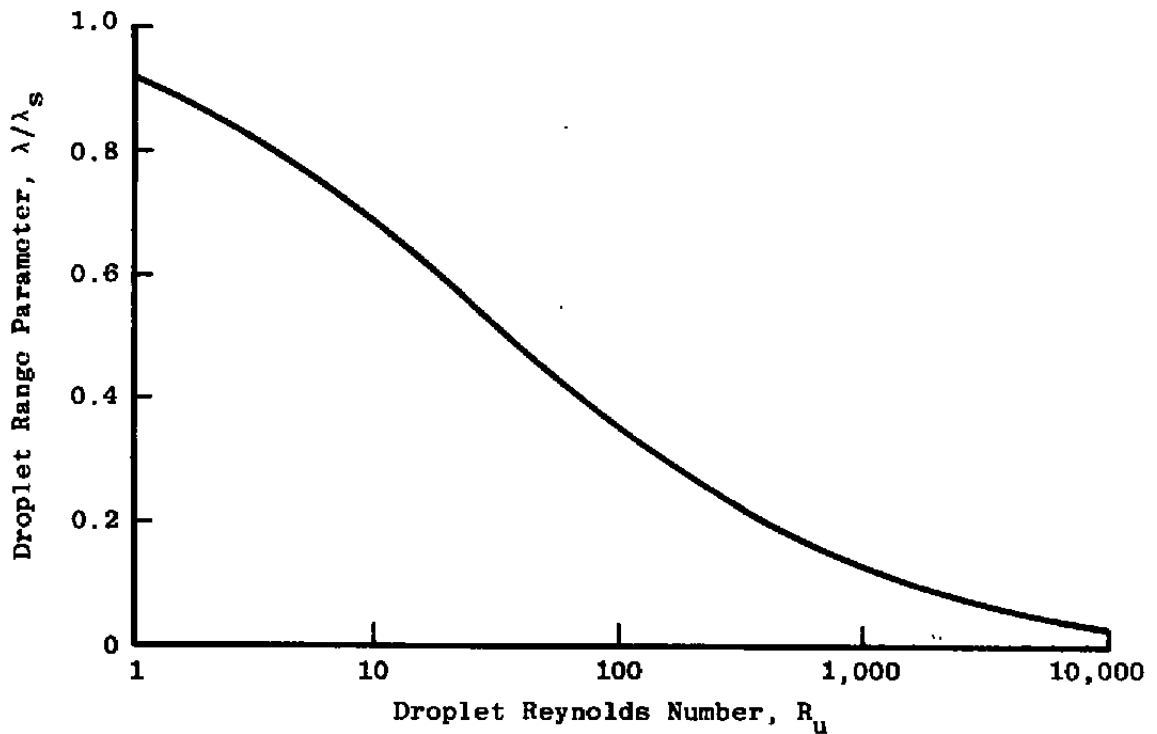


Figure A-1. Droplet range parameter versus Reynolds number.

## APPENDIX B

### DERIVATION OF THE ICING ENERGY EQUATION

#### DEFINITION OF THE CONTROL VOLUME

The control volume to be analyzed is located along the stagnation line and extends from outside the boundary layer to the surface of the body as shown in Fig. B-1. It encloses a distance  $\Delta s$  along the external surface and, for dimensional completeness, extends one unit length in the spanwise direction (into the page).

#### MASS BALANCE ON AN ICING SURFACE

An evaluation of all the mass entering and leaving the control volume is shown in Fig. B-2. A mass balance equation can be formed from these terms and is given below.

$$W_w \Delta s - W_e \Delta s - w_r = W_i \Delta s \quad (\text{B-1})$$

There will be no water inflow along the surface because a stagnation-point control volume has been selected.

Since the freezing fraction is defined as the proportion of the total mass of liquid entering the control volume that freezes in that control volume, it can be expressed by the following equation:

$$n = \frac{W_i}{W_w} \quad (\text{B-2})$$

By substituting Eq. (B-1) into Eq. (B-2), the water flow out of the control volume can be expressed as

$$w_r = (1 - n) W_w \Delta s - W_e \Delta s \quad (\text{B-3})$$

#### ENERGY BALANCE ON AN ICING SURFACE

The same control volume concept is used to formulate the energy balance on the icing surface. In words, the First Law of Thermodynamics for a control volume can be expressed as

$$\text{energy inflow rate} = \text{energy outflow rate} + \text{energy storage rate}$$

The modes of energy transfer, illustrated in Fig. B-3, are as follows:

Mode of Energy Transfer	Energy Flow Rate
1. impinging water	$W_w i_{w,T} \Delta s$
2. evaporation	$W_e i_{v,sur} \Delta s$
3. water flow out of control volume	$w_r i_{w, sur}$
4. ice accumulation	$W_j i_{i,sur} \Delta s$
5. convection	$q_c \Delta s$
6. conduction through skin	$q_K \Delta s$

Using the convention that energy flow into the control volume is positive, the terms can be summed to yield the energy equation.

$$W_w i_{w,T} \Delta s = W_e i_{v,sur} \Delta s + w_r i_{w,sur} + W_j i_{i,sur} \Delta s + q_c \Delta s + q_K \Delta s \quad (B-4)$$

The evaluation of the terms of the energy equation has been done by various authors, most notably by Sogin (Ref. B-1), Lowzowski et. al. (Ref. B-2), and Cansdale and Gent (Ref. B-3). The following sections will evaluate each of the terms, highlighting differences from previous models. The references should be consulted for further details.

## IMPINGING WATER

Since the droplets are essentially brought to rest when they strike an object, it is appropriate to use the stagnation enthalpy defined as

$$i_{w,T} = c_{p_{w,s}} (T_s - 32) + \frac{U_\infty^2}{2g_c J} \quad (B-5)$$

The arbitrary reference for zero enthalpy used in this study is water at 32°F. Substituting Eq. (B-5), the energy flow rate of the impinging water becomes

$$W_w i_{w,T} \Delta s = W_w \left[ c_{p_{w,s}} (T_s - 32) + \frac{U_\infty^2}{2g_c J} \right] \Delta s \quad (B-6)$$

## EVAPORATION

The rate of energy transfer from the surface because of evaporation is given by

$$W_e i_{v,sur} \Delta s = W_e [c_{pw,sur} (T_{sur} - 32) + L_v] \Delta s \quad (B-7)$$

where  $W_e$  is the evaporative mass transfer rate and  $L_v$  is the latent heat of vaporization.

The mass transfer rate is analogous to the convective heat-transfer rate and can be written as

$$W_e = g \Delta B \quad (B-8)$$

where  $g$  is the mass transfer coefficient and  $\Delta B$  is the evaporative driving potential. The mass transfer coefficient,  $g$ , can be evaluated using the analogy to heat transfer given by the equation

$$g = \frac{h_c}{c_{pa}} \left( \frac{Pr}{Sc} \right)^{0.667} \quad (B-9)$$

where  $Pr$  is the Prandtl number and  $Sc$  is the Schmidt number.

The mass transfer driving potential is analogous to the temperature difference in the convective heat-transfer equation. In the case of evaporation, the driving potential is a vapor concentration difference instead of a temperature difference. The equation used in this study is similar to that derived by Sogin (Ref. B-1) and given as

$$\Delta B = \frac{P_{v,s}/T_s - (P_T/T_T) P_{v,s}/P_s}{(1/0.622) P_T/T_T - P_{v,s}/T_s} \quad (B-10)$$

This term accounts for compressibility effects as does the term derived by Cansdale in Ref. B-3.

## WATER FLOW OUT OF THE CONTROL VOLUME

The water flowing out of the control volume will be at the surface temperature, allowing the enthalpy to be expressed as

$$i_{w,sur} = c_{pw,sur} (T_{sur} - 32) \quad (B-11)$$

Using Eq. (B-3), the runback water energy flow rate can be expressed as

$$w_r i_{w,sur} = [(1 - n) W_w \Delta s - W_e \Delta s] c_{pw,sur} (T_{sur} - 32) \quad (B-12)$$

## ENERGY OF THE ICE ACCUMULATION

From the definition of the freezing fraction, Eq. (B-2), the freezing rate is

$$W_i \Delta s = n W_w \Delta s \quad (\text{B-13})$$

The enthalpy of ice referenced to water is 32°F is

$$\dot{i}_{i,\text{sur}} = c_{p_i,\text{sur}} (T_{\text{sur}} - 32) - L_f \quad (\text{B-14})$$

Combining Eq. (B-13) into Eq. (B-14), the energy storage rate in the control volume can be expressed as

$$W_i \dot{i}_{i,\text{sur}} \Delta s = n W_w [c_{p_i,\text{sur}} (T_{\text{sur}} - 32) - L_f] \Delta s \quad (\text{B-15})$$

## NET CONVECTIVE HEAT FLUX

Convective heat flow rate is normally defined by the following equation:

$$q_c \Delta s = h_c \Delta T \Delta s \quad (\text{B-16})$$

In an icing analysis,  $\Delta T$  is the difference between the surface temperature and the adiabatic wall temperature and can be expressed by following equation:

$$\Delta T = T_{\text{sur}} - T_{\text{aw}} \quad (\text{B-17})$$

The adiabatic wall temperature,  $T_{\text{aw}}$ , is given by

$$T_{\text{aw}} = T_L \left( 1 + r_c \frac{\gamma - 1}{2} M_L^2 \right) \quad (\text{B-18})$$

where  $T_L$  and  $M_L$  are the temperature and Mach number at the edge of the boundary layer, respectively, and  $r_c$  is the recovery factor. At the stagnation point,  $T_L$  is equal to the total temperature,  $T_T$ , and  $M_L = 0.0$ . The total temperature can be expressed in terms of the free-stream velocity as

$$T_T = T_s + \frac{U_{\infty}^2}{2g_c c_{p_n}} \quad (\text{B-19})$$



Substituting Eqs. (B-17), (B-18), and (B-19) into Eq. (B-16), the expression for the convection heat flow rate becomes

$$q_c \Delta s = h_c \left[ T_{sur} - T_s - \frac{U_\infty^2}{2g_c J c_{pa}} \right] \Delta s \quad (B-20)$$

The heat-transfer coefficient for the stagnation line of a cylinder and the leading edge of airfoils is given in Ref. B-4 as

$$h_c = \frac{1.14 (Re)^{0.5} (Pr)^{0.4} k}{c} \quad (B-21)$$

where Re is the free-stream Reynolds number and c is the cylinder diameter or, in the case of an airfoil, the leading-edge diameter.

A more general derivation of this term is given in Ref. B-2

## CONDUCTION INTO THE SKIN

When the cloud is first encountered, a temperature difference will exist between the wetted surface and the inner structure of the skin which was at an equilibrium temperature prior to entering the cloud. The evaluation of the resulting conductive heat flow rate is dependent on knowing the thermal conductivity and detailed geometry of the skin. The calculation of this heat flow rate through what could be a complicated composite structure is avoided in scaling studies by requiring that the objects have the same internal structure and are made of identical materials. It is then assumed that the conductive heat flow rate between the model and full-scale will be identical, i.e.

$$q_K (\Delta s)_{model} = q_K (\Delta s)_{full-scale}$$

To simplify the solution of the energy equation,  $q_K \Delta s$  is dropped from the equation. This will not change the values of any of the calculated similitude conditions but may effect the absolute value of the calculated surface temperature and freezing fraction.

The energy terms can now be summed to form the complete energy balance equation for a stagnation-line control volume.

$$\begin{aligned}
W_w \left[ c_{p_{w,s}}(T_s - 32) + \frac{U_\infty^2}{2g_c J} \right] &= W_e \left[ c_{p_{w,sur}}(T_{sur} - 32) + L_v \right] \\
+ [(1 - n) W_w - W_e] c_{p_{w,sur}}(T_{sur} - 32) &+ n W_w [c_{p_{i,sur}}(T_{sur} - 32) - L_f] \quad (B-22) \\
+ h_c \left[ T_{sur} - T_s - \frac{U_\infty^2}{2g_c J c_{p_a}} \right] &
\end{aligned}$$

Note that the control volume surface length,  $\Delta s$ , has been cancelled uniformly from each term of the energy equation.

### REFERENCES

- B-1. Sogin, H. H. "A Design Manual for Thermal Anti-Icing Systems." Illinois Institute of Technology, WADC-TR-54-313, December 1954.
- B-2. Lozowski, E. P., Stallabrass, J. R., and Hearty, P. F. "The Icing of an Unheated Nonrotating Cylinder in Liquid-Water Droplet-Ice Crystal Clouds." National Research Council of Canada (NCR) Report LTR-LT-88, February 1979.
- B-3. Cansdale, J. T. and Gent, R. W. "Ice Accretion on Aerofoils in Two-Dimensional Compressible Flow—A Theoretical Model." Royal Aircraft Establishment Technical Report 82128, January 1983.
- B-4. Kreith, F. *Principles of Heat Transfer*. Intext Educational Publishers, New York, 1973 (Third Edition).

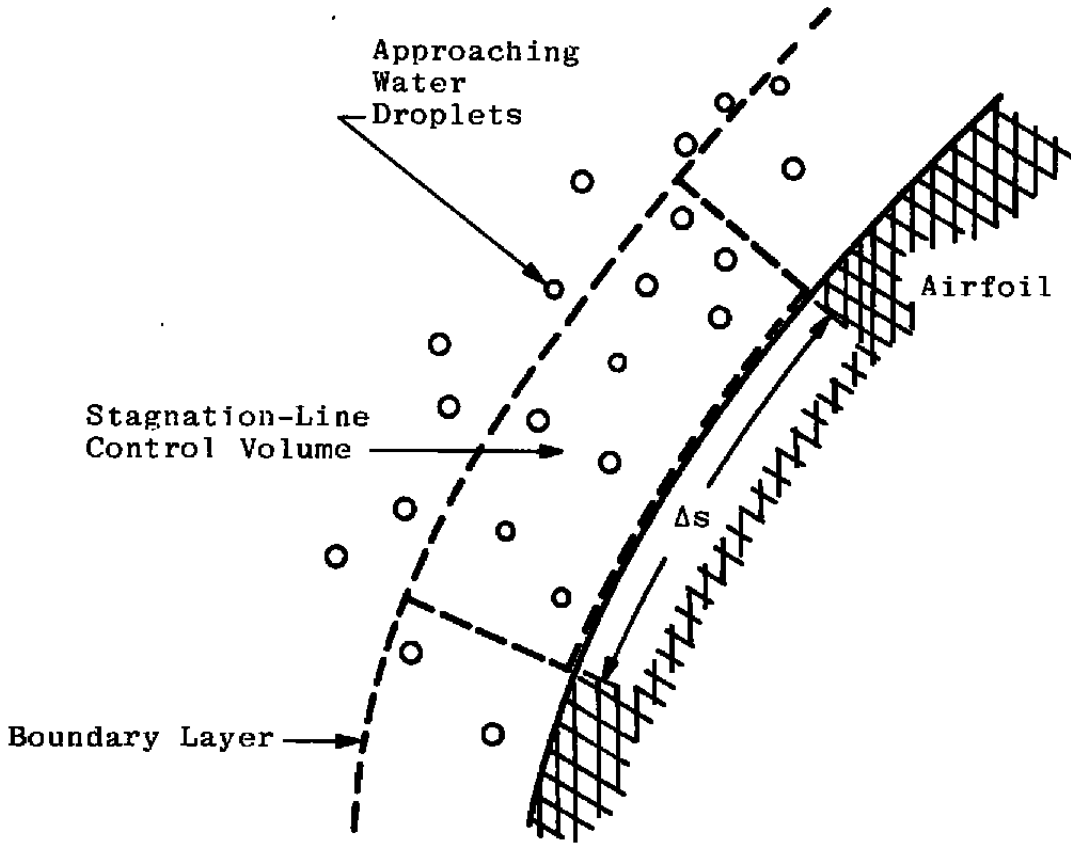


Figure B-1. Identification of a stagnation-line control volume.

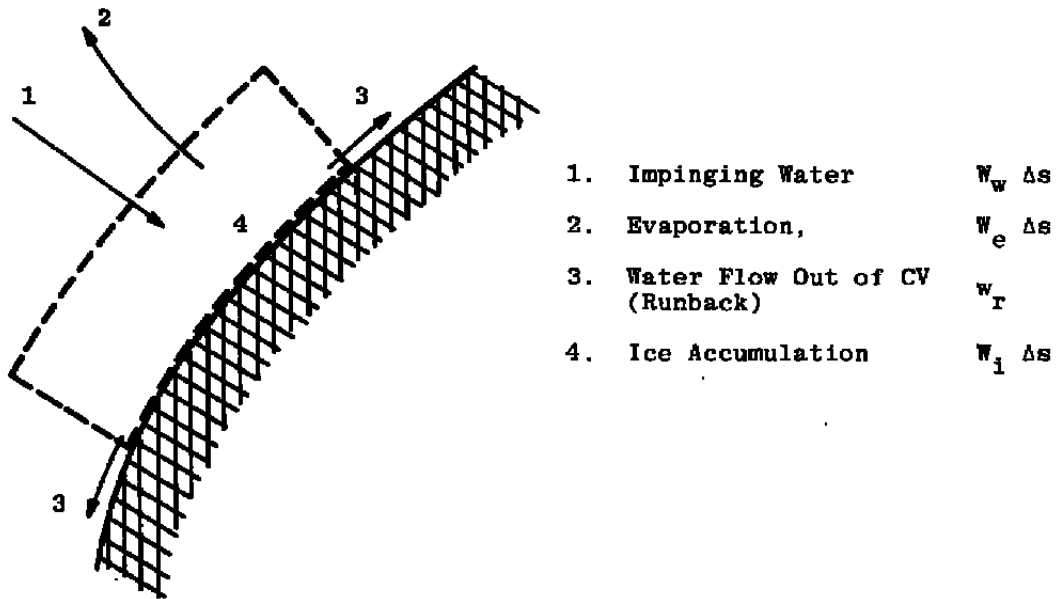


Figure B-2. Mass balance for a stagnation-line control volume.

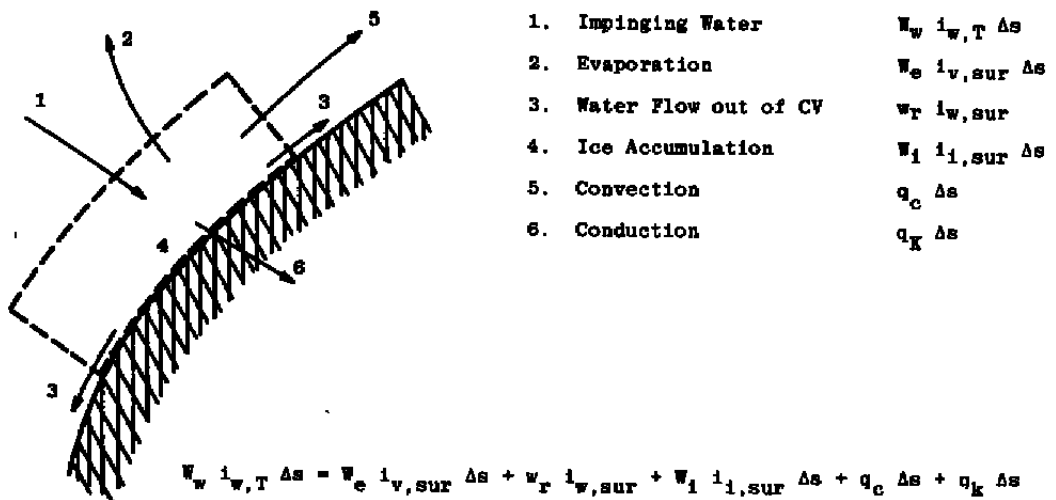


Figure B-3. Energy balance for a stagnation-line control volume.

## NOMENCLATURE

$A_c$	Accumulation parameter
$\Delta B$	Mass transfer driving potential
$b$	Relative heat factor
$C_D$	Drag coefficient
$c$	Characteristic length
$c_p$	Specific heat, Btu/lbm
$D$	Drag force, lbf
$d$	Droplet diameter, ft unless specified
$\bar{d}_m$	Mass median droplet diameter, ft unless specified
$E_m$	Total collection efficiency
$F$	Equivalent force, lbf
$g$	Mass transfer coefficient, lbm-°F/Btu
$g_c$	Constant, 32.174 lbm-ft/lbf-sec <sup>2</sup>
$H$	Projected height, ft
$h$	Convective heat-transfer coefficient, Btu/ft <sup>2</sup> /hr/°F
$i$	Enthalpy, Btu/lbm
$J$	Mechanical equivalent of heat, 778 ft-lbf/Btu
$K$	Inertia parameter
$K_0$	Modified inertia parameter
$\bar{K}$	Particle scaling parameter

<b>k</b>	<b>Thermal conductivity, Btu/ft/hr/°F</b>
<b>L<sub>f</sub></b>	<b>Heat of fusion, Btu/lbm</b>
<b>L<sub>v</sub></b>	<b>Heat of vaporization, Btu/lbm</b>
<b>LWC</b>	<b>Liquid-water content, g/m<sup>3</sup></b>
<b>M</b>	<b>Mach number; Moment, ft-lbf</b>
<b>m</b>	<b>Mass, lbm</b>
<b>m''</b>	<b>Mass per unit area, lbm/ft<sup>2</sup></b>
<b>n</b>	<b>Freezing fraction</b>
<b>P</b>	<b>Pressure, psia</b>
<b>Pr</b>	<b>Prandtl number</b>
<b>q</b>	<b>Dynamic pressure, psia</b>
<b>q<sub>c</sub></b>	<b>Convective heat flux, Btu/ft<sup>2</sup>/hr</b>
<b>q<sub>K</sub></b>	<b>Conductive heat flux, Btu/ft<sup>2</sup>/hr</b>
<b>R</b>	<b>Droplet Reynolds number based on <math> U_a - U_d </math></b>
<b>Re</b>	<b>Free-stream Reynolds number</b>
<b>R<sub>u</sub></b>	<b>Droplet Reynolds number based on <math>U_\infty</math></b>
<b><math>\mathcal{R}</math></b>	<b>Reynolds number integration variable</b>
<b>r</b>	<b>Droplet radius, ft</b>
<b>s</b>	<b>Surface length, ft</b>
<b><math>\Delta s</math></b>	<b>Surface length increment, ft</b>

<b>Sc</b>	<b>Schmidt number</b>
<b>T</b>	<b>Temperature, °F</b>
<b>t</b>	<b>Time, sec</b>
<b><math>U_{\infty}</math></b>	<b>Velocity, fps</b>
<b>W</b>	<b>Mass flux, lbm/ft<sup>2</sup>/sec</b>
<b>w</b>	<b>Mass flow rate, lbm/sec</b>
<b>x</b>	<b>Length integration variable, ft</b>
<b><math>y_0</math></b>	<b>Vertical distance between tangent trajectory release points, ft</b>
<b><math>\beta</math></b>	<b>Local collection efficiency</b>
<b><math>\gamma</math></b>	<b>Slope of log <math>C_D</math> versus log R curve; ratio of the specific heats of air = 1.4</b>
<b><math>\theta</math></b>	<b>Air energy transfer potential, °F</b>
<b><math>\lambda/\lambda_s</math></b>	<b>Droplet range parameter</b>
<b><math>\mu</math></b>	<b>Viscosity, lbf-sec/ft<sup>2</sup></b>
<b><math>\rho</math></b>	<b>Density, lbm/ft<sup>3</sup></b>
<b><math>\sigma</math></b>	<b>Shear stress, lbf/ft<sup>2</sup></b>
<b><math>\tau</math></b>	<b>Icing time, sec unless specified</b>
<b><math>\phi</math></b>	<b>Droplet energy transfer potential, °F</b>

**Subscripts**

<b>a</b>	<b>Air</b>
<b>aw</b>	<b>Adiabatic wall</b>

<b>c</b>	<b>Critical</b>
<b>d</b>	<b>Droplet</b>
<b>e</b>	<b>Evaporation, evaporative</b>
<b>i</b>	<b>Ice</b>
<b>l</b>	<b>Lower surface</b>
<b>L</b>	<b>Condition at the edge of the boundary layer</b>
<b>r</b>	<b>Runback water</b>
<b>s</b>	<b>Static condition</b>
<b>sur</b>	<b>Surface condition</b>
<b>T</b>	<b>Total condition</b>
<b>u</b>	<b>Upper surface</b>
<b>v</b>	<b>Vapor</b>
<b>w</b>	<b>Liquid water</b>
<b><math>\infty</math></b>	<b>Free-stream condition</b>

**Superscript**

<b>'</b>	<b>Nondimensionalized parameter</b>
<b><math>\rightarrow</math></b>	<b>Vector quantity</b>